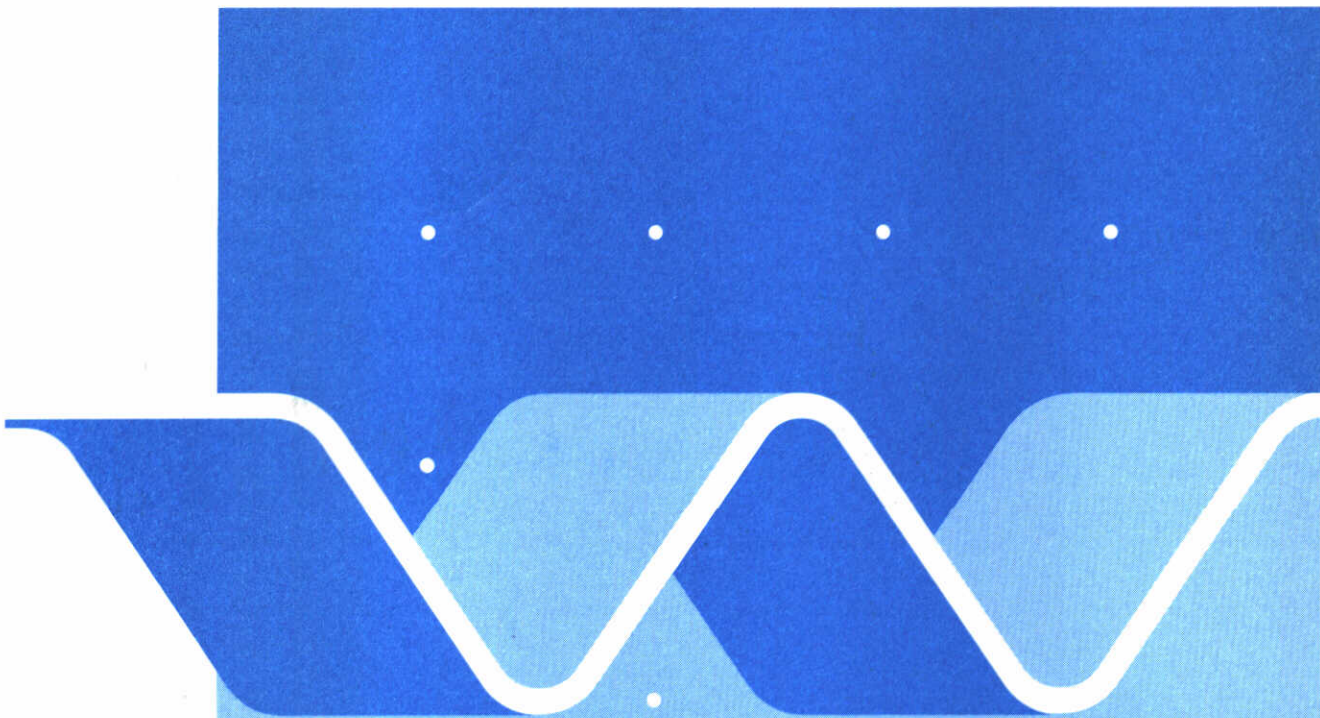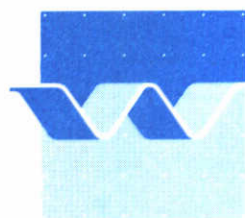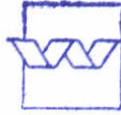# Verification of numerical wave propagation models with laboratory measurements

HISWA verification in the directional wave basin

delft hydraulics

Verification of numerical wave propagation models with laboratory measurements

HISWA verification in the directional wave basin

M.W. Dingemans

CONTENTS

Part 1a : TEXT

Part 1b : APPENDICES A-G

Part 1c : APPENDICES H-V

Part 1d : FIGURES

LIST OF FIGURES

LIST OF FIGURES (continued)

LIST OF FIGURES (continued)

1. Introduction.

The Delta Department of Rijksvaterstaat commissioned Delft Hydraulics a verification study of the spectral refraction programme HISWA against laboratory measurements (letters WT 449, 4 June 1985 and WT 309, 18 September 1986). As the research has been carried out in a joint project of Rijksvaterstaat and Delft Hydraulics, about half of the costs were furnished by Delft Hydraulics. The HISWA model has been devised by the University of Technology Delft, under contract of Rijksvaterstaat. As the program HISWA differs from other available wave propagation programs, especially in accounting for the directional spread of the wave fields, the new facility at Delft Hydraulics, in which two-dimensional spectra can be generated in a wave basin, was to be used for the verification study. The measurements have been carried out by A. Turkenburg under direction of J. Bosma. The program HISWA was run by P. Groenevoud and J. Koopmans, under the direction of M.W. Dingemans, who carried out most of the verification. The project management was carried out at Rijksvaterstaat by J.A. Vogel and at Delft Hydraulics by M.J.F. Stive.

The purpose of the present report is a limited one, as the most interesting results have been presented at the Int. Conference on Coastal Engineering at Taipei (see, Dingemans et al., 1986). This paper has been included as appendix A. The purpose of the present report is foremost to give details on the measurements, the computations and the comparisons for future reference, whereas a detailed discussion of each resulting verification is not given. In a sense the present report is to be viewed as a supplement to the paper of Dingemans et al. (1986). A second purpose of this report is to give the results of the measurements to be able to use for future purposes.

The plan of the report is as follows. For the scope of the study is referred to Appendix A. In chapter 2 the realisation of the study is described; here the set-up of the measurements and the chosen bottom geometry are described and the choice of the measurement programme is discussed. Furthermore the data handling and the reduction into parameters to be compared with computed parameters are discussed.

In chapter 3 the results of the confrontation of computations with the respective measurements are given and the correspondence is expressed by a set

of statistical parameters. The performance of HISWA has been discussed in terms of the prediction of several wave parameters as wave height, wave period, wave direction and directional spread. For the computations two geometries have been chosen, a simple one and a more difficult one. For a few cases also computations with the parabolic wave propagation model CREDIZ have been performed; these computations have been performed in order to get some notion of the performance of HISWA in relation to the performance of other wave propagation programs. The intercomparison of the CREDIZ results and the measurements and the corresponding HISWA results is discussed in chapter 4.

As the opportunity to measure wave-induced currents for a few of the measurement conditions has been made available as part of the applied research programme of Rijkswaterstaat (TOW), some discussion on the wave-induced current computation has been given in chapter 5. It is remarked that the effect of these wave-induced currents on the wave field has been shown to be appreciable, see Appendix A and chapter 3. The summary, conclusions and recommendations are given in chapter 6.

A large number of appendices with details of results of measurements and computations have been added. The appendices comprise information on the geometry and results of the measurements, detailed results of the computations (wave height, wave period, wave direction and directional spread), at the chosen 26 sites, and appendices concerning the intercomparison of computed and measured parameters. The results for the computations have been given in such great detail because it can be imagined that in subsequent versions of the HISWA programme slightly different results may be obtained; the differences may then be ascertained. For use in projects the relation with the mean wave frequency as used in HISWA and the peak frequency in the spectrum has been given for a number of spectral forms in appendix G and the measure of the directional spreading for the spectral spreading function as used in HISWA has been given in appendix F for a number of directional distributions. Furthermore some comments on the averaging in HISWA, as defined in appendix A, have been given in appendix T. The comparison of the effect of wave dissipation in HISWA and in models based on the peak frequency has been commented upon in appendix U.

It has to be remarked that the HISWA computations as reported here were all

carried out in 1986 with the version of the program as was installed at the Rijkswaterstaat Data Processing Department (DIV) SPERRY computer and was maintained by the department Dienst Getijdewateren (DGW) of Rijkswaterstaat.

The present report comes in four volumes:

    part 1a : text, (this volume)
    part 1b : appendices A-G,
    part 1c : appendices H-V, and
    part 1d : Figures.

The investigations have been carried out by M.W. Dingemans, who also wrote this report.

2. Realisation of the study.

2.1 Introduction.

This chapter serves as a description of the measurements and the experimental procedure and the data processing techniques used. Furthermore, the method of verification is discussed. For a clear understanding of the set-up of the measurements, at first the barest essentials of the HISWA model are discussed in section 2.2. Subsequently, the chosen bottom geometry and the positions of the measuring devices are discussed in section 2.3. The measuring program is given in section 2.4 and the experimental procedure and the instruments are described in section 2.5. The data collection and the data processing techniques used are given in section 2.6. Because of the special definition of the mean wave period used in HISWA, it has been necessary to obtain the corresponding wave period from the measured wave spectra; at 7 of the 26 measuring sites the corresponding wave period measures have been determined from the measured spectra, along with some other spectral wave period measures; this is discussed in section 2.7. The ways in which the verification is performed for the various aspects is described in section 2.8. The procedure for the current measurements is described in section 2.9.

2.2 Some properties of the HISWA model.

HISWA is a wave propagation model in which the wave action is not only a function of place (x, y), but also of the wave direction θ : $A = A(x, y, \theta)$. The wave propagation part is based on the geometrics optics approach, while also current refraction can be accounted for. The HISWA computation proceeds with one frequency, ω, a change in characteristic frequency due to wave dissipation resulting from wave breaking or bottom friction and due to wave growth due to wind has been modeled. The mathematical model has been given on the second page of Appendix A in a very concise form; it is seen there that the mathematical model of HISWA in fact consists of two differential equations, one for the wave action $A(x, y, \theta)$ and one for the frequency θ. Source terms describing wave dissipation, frequency change and wave growth due to wind are collected in the right-hand sides of these two differential equations. A general discussion of these source terms can be found in Holthuijsen and Booij (1986) and a more detailed description of

the present state of modeling of these terms is not yet available; but such a description is foreseen by Booij and Holthuijsen, where also the numerical approach will bedescribed.

The physical effects which are modeled in HISWA are :

- Bottom and current refraction;
- directional spreading;
- dissipation due to bottom friction;
- dissipation due to wave breaking;
- diffraction by some ad-hoc method;
- wave blocking due to large currents;
- frequency changes due to dissipation and wind.

2.3 The bottom geometry and the measuring positions.

Requirements for the experiments.

In previous verification studies as discussed in Dingemans (1985) only scarce information on directional spread is available; in HISWA the modeling of effects of directional spread is especially new to the previous verified models. Therefore the laboratory experiment has been set up such that effects of directional spreading may be studied. Care has been exercised that also effects of frequency change due to dissipation become available. However, it has to be noted that for a separate study of frequency changes due to dissipation an experiment in a wave flume is better suited because much longer wave flumes are available than is possible for the extent of wave basins.

A first requisite of a wave propagation model is that the wave heights are correctly predicted in some region of space. As we are primarily interested in nearshore regions where much reduction in wave height occurs due to wave breaking, it is necessary to verify HISWA also for situations in which dissipation due to wave breaking is present. As basis for the wave breaking modeling has been taken the now well proven one-dimensional model of Battjes and Janssen (1978), see also Battjes and Stive (1985), but now adapted for directional spreading.

The effect of directional spreading of the wave field has to be studied for situations where also a fair amount of refraction is present. This is also of importance because it is well known that the geometric optics approxima- tion is very sensitive for small localized bottom disturbances (see exam- ples in Dingemans, 1985); the idea is that in presence of directional spreading these akward effects are somewhat averaged out, sothat the resul- ting wave field becomes more robust for small bottom perturbations with accounting for directional spreading than it is without. It is to be noted that in HISWA only one characteristic frequency is considered, albeit pos- sibly different for the various wave directions; for a truly two-dimensio- nal wave spectrum the averaging effects are larger, consider, e.g., possi- ble caustics in regions of space with irregular iso-baths.

The chosen bottom geometry.

Considering above requirements for the measurements, and given the maximum extents of a new wave basin facility at Delft Hydraulics (for a descrip- tion, see Mynett et al., 1984), the geometry of Figure 1 was decided upon after studying a few close variants numerically. It consists of a submerged semi-cylindrical bar with a well rounded head over which considerable re- fraction may be expected. This bar is placed on an otherwise horizontal bottom with undisturbed water depth of 40 cm. For a detailed description of the geometry of the bar is referred to Appendix B. This undisturbed depth has been chosen such that for the undisturbed depth no extra friction and capillary wave effects would be encountered. Moreover, in front of and behind the bar propagation distance of a few wave lengths is still availa- ble. At least some effect of the characteristic frequency change may be studied, although larger propagation distances would be preferably for that purpose. The essential dimensions of the wave basin are given on the third page of Appendix A.

In order to have a check on the behaviour of the wave basin, also the sim- pler geometry of a fully cylindrical bar extending towards the opposite side wall has been studied. And in order to have a thorough check on the wave generation devices, also measurements without any bar have been per- formed; this case is denoted by 'empty basin'.

The measuring positions.

The coordinate system in the wave basin was chosen with the origin in the middle of the wave generator in its rest position. The x-axis is taken perpendicular to the generator and the y-axis is taken along the wave board, see Figure 2. Wave height gauges were placed in lines perpendicular and parallel to the wave board. Lines x = constant are indicated by numbers and lines y = constant are indicated by letters. The coordinates of the measuring positions and the various lines are indicated in Table 2.1 below. The instruments used were 7 wave-gauges and 3 wave-direction meters. To cover all measuring positions, three successive tests for the same input condition were necessary; here instruments at two positions were kept fixed, at position 10 a wave direction meter was kept and at position 15 a wave gauge was kept fixed. This enabled us to check the similarity of the repetitions. The measuring postions are numbered according to 1) the number of the test run and 2) the instrument used; the wave-gauges are numbered 1 to 7 and the wave direction meters are numbered 8, 9 and 0. See also appendix S.

line	x [m]						
7	22.5	27		39		29	28
6	19.5			35		15	25
5	18.0			34	38	14	24
4	15.0	17	37	33		13	23
3	12.0			32		12	22
2	7.5	16		31		11	21
1	2.0	19				10	18
	<-- y [m]	10	5.5	2.5	1.25	0	-5
	line	a	b	c	d	e	f

Table 2.1 The positions (x,y) of the measuring instruments.

As the coordinates x and y are not mentioned in the Tables below, the positions are also given in the following form:

27		39		29	28
		35		15	25
		34	38	14	24
17	37	33		13	23
		32		12	22
16		31		11	21
19				10	18

Table 2.2 The codes of the measuring positions (sites).

The considerations for chosing the measuring postions as described above are as follows.

- Along the whole of the wave board the input two-dimensional spectrum has to be defined and the variability along the wave generator should be known. Therefore three wave-direction meters are placed at line 1. One instrument has been placed in the middle of the wave board on a short distance from the flaps and two others are placed asymmetrically at line 1. Point 18 was chosen to lie on line f which intersects the cylindrical part of the bar about in the middle and point 19 was chosen such that on line a the depth is constant (.40 m).

- Line 2 is chosen such that measuring positions just before the bar become available.

- Lines 3 and 5 are situated such that on the slopes of the bar wave information becomes available, and line 4 is situated above the smallest depth.

- Line 6 is situated just behind the bar.

- Line 7 is some distance behind the bar, but not too close to the toe of the gravel beach. Here three wave direction meters are placed to be able to identify the refraction effects of the head of the construction and the different directional spreading, also in conjunction with different wave dissipation along the different wave paths.

- Line a is chosen to have constant depth values.

- Line f has been introduced to have information on wave dissipation characteristics, and is situated such that for a large part no two-dimensional effects are to be expected.

- Line e serves to study the influence of the head of the construction on the cylindrical part of the bar.

- Line c is situated to cross the head of the construction.

- On both lines b and d only one instrument is placed, so as to get a good coverage of the head of the construction. At point 38 the directional wave-instrument has been placed to have a check on the computed wave directions; initial computations showed that here the largest refraction effects occurred.

2.4 The measurement program.

A measuring program has been defined in such a way that the various aspects of the verification can be studied. In terms of the properties of the two-dimensional spectrum $S(f,\theta)$ the conditions are varied according to:

- the width of $S(f,\theta)$ in f;
- the width of $S(f,\theta)$ in θ;
- the wave height HmO;
- the incident wave direction θ_o .

The two-dimensional spectrum is written as

$$S(f,\theta) = E(f).D(\theta;f),$$

where for $E(f)$ spectra of the JONSWAP-type are taken and for $D(\theta;f)$ is taken a $\cos^m \theta$-type directional distribution :

$$E(f) = A_o \tilde{S}(\nu) \quad , \quad \tilde{S}(\nu) = \nu^{-5} \exp\left[-\frac{5}{4}\nu^{-4}\right] \gamma(\nu)$$

$$\gamma(\nu) = \gamma_o \exp\left[-\frac{(\nu-1)^2}{2\sigma^2}\right] \quad , \quad \nu = f/f_m$$

$$A_o = \alpha_o g^2 (2\pi)^{-4} f_m^{-5} ; \quad \sigma = 0.07, \ \nu \leq 1; \quad \sigma = 0.09, \ \nu > 1$$

and

$$D(\theta;f) = B_2 \cos^m(\theta-\theta_0); \quad -\frac{\pi}{2} \le \theta-\theta_0 \le \frac{\pi}{2}$$

$$= 0 \quad ; \quad \text{elsewhere,}$$

with

$$B_z = \frac{1}{\sqrt{\pi}} \frac{\Gamma(\frac{1}{2}m + 1)}{\Gamma(\frac{1}{2}m + \frac{1}{2})} .$$

Here γ_0 is the peak-enhancement factor and m is the exponent of the $\cos^m\theta$ directional distribution. The input conditions have been chosen in such a way that some of the cases may also be useful for testing of other wave propagation programs. The conditions have been chosen as given in Table 2.3.

case	HmO	Tp	γ_0	m	θ_0	current meas.
	[cm]	[s]			[deg.]	
1	5	1.25	7	20	0	-
2	10	1.25	7	20	0	-
3	10	1.25	7	4	0	-
4	10	1.25	1	4	0	-
5	10	1.25	3.3	4	0	+
6	10	1.25	7	20	20	-
7	10	1.25	3.3	4	20	-
8	10	1.25	3.3		0	+

Table 2.3 Input conditions.

The cases 2 and 5 are considered to be the primary cases around which the parameters are varied. Case 2 is the case of a two-dimensional spectrum narrow in both the frequency (a large value γ_0 and direction (a large exponent m). The characteristic width of the directional distribution is for m=20 12.5° and for m=4 it is 25°, see Appendix F for definitions of directional spread and for numerical examples. The considerations leading to the above choice of measuring program are as follows.

- Case 5 is to be viewed as the most commonly occurring one in nature, a mean JONSWAP-type of spectrum and a reasonable width of the directional distribution. An exponent m = 2 is also much mentioned, but this leads to a spread of 32.5° and a not too large spread seems to be advisable for using in a wave basin, especially when considering wave reflection due to the side walls.

- Case 2 is to be seen a the archetype of a narrow spectrum both in frequency and direction. The narrowness in frequency is shown in Fig. 3, where non-dimensionalized JONSWAP spectra with γ_o = 3.3 and γ_o = 7 are plotted together. The difference in directional spread of 25.5 and 12.5°, belonging to m = 4 and m = 20 respectively, should be sufficient in order to measure significant differences. The directional distributions $B_2 \cos^m \theta$ are shown in Figures 4a and 4b for the combinations m = 4, m = 20, m = 64 and for m = 2, m = 4, m = 8 respectively.

- Case 2 is especially suited for testing the behaviour of mono-chromatic, mono-directional wave propagation models, such as, e.g., the parabolic wave propagation model or refraction models where wave dissipation has been taken into account such as VELD (see Dingemans, 1985). Moreover, while HISWA has been modeled with normal sea conditions in mind, the mathematical description of HISWA is such that also cases with narrow directional distributions can be computed.

- The cases 1, 3 and 4 constitute simple variations of the two fundamental cases 2 and 5. The difference between cases 1 and 2 is the low wave height in case 1, for which case not much wave breaking is to be expected and therefore the effect of wave dissipation on the resulting directional wave characteristics may be obtained from a comparison of cases 1 and 2. Case 1 is the only case for which wave dissipation is not dominant.

- Case 3 has a wide directional distribution, but a narrow frequency distribution, a situation which is expected not to occur very often in nature; this case allows studying the effect of directional spread alone by comparing it with case 2.

- Case 4 is the case of both wide frequency and directional distributions. For E(f) is taken the Pierson-Moskovitz spectrum. The effect

of differences in width in frequency, given a wide directional distribution, can be obtained by comparing case 4 with the "standard JONSWAP case", case 5.

- Case 8, the case of the mean JONSWAP spectrum, without directional spreading, is chosen as a check on the method of generation of directional waves in the basin.

- Cases 6 and 7 are the two cases where the principal wave direction is not perpendicular to the wave generator, but has an angle of 20° with the x-axis in positive direction (according to the mathematical definition). For these cases more reflection is to be expected from the leftern sidewards boundary. The effect of oblique waves can be studied for case 6 by comparing the results with those of case 2 and for case 7 by comparing with case 5.

With regard to the current measurements, to be described in Appendix D, the primary case is case 5, with the mean JONSWAP spectrum and a wide directional distribution. In order to study the possible necessity of performing morphological experiments in directional wave basins, for the case without directional spreading, case 8, also current measurements are performed. The measurements for the three bottom geometries and the eight input conditions are often denoted by mexy, where x=1 denotes the empty basin, x=2 denotes the fully cylindrical bar geometry and x=3 denotes the semi-cylindrical bar geometry. There is y=1 to y=8 denoting the input conditions as defined in Table 2.3. So is me35 the measurement for the semi-cylindrical bar and input condition 5, while me13 denotes the measurements for the same case 5 for the empty basin. All measurements for the semi-cylindrical bar geometry are indicated by me3x.

2.5 Instruments and experimental procedure.

The measuring instruments used consisted of 7 wave height gauges, used at 19 measuring positions (denoted by the full circles in Figure 2) and 3 wave directional meters used at 7 measuring positions (the circles with crosses in Figure 2). The specifications of these instruments are as follows.

Wave gauge.

The water surface elevation was measured with a resistance type, tempera-
ture corrected wave gauge. The relationship between the depth of immersion
of the vertical conductor and the output voltage is aprroximately linear.
The deviation from linearity is less than 1 % (relative error).

Wave direction meter GRSM.

In order to detect the wave directionality, Delft Hydraulics has developed
a wave direction meter in which a wave gauge as described above is combined
with point measurement of two perpendicular orbital velocity components in
the horizontal plane. The device for these velocity measurements is a
button-type instrument containing two orthogonal electro-magnetic velocity
meters, see Fig. 5. The stability is approximately 1 cm/s, the noise is
better than 1 cm/s and the linearity deviation is less than 1 % (relative
error). The instrument was placed such that the direction of the two
velocity components was +45° and -45° with the x-axis (the line perpendi-
cular to the wave generator in rest). The velocity components have been
measured at 22 cm above the local bottom.

The wave generator.

The wave pattern can be built up out of 120 Fourier components, each with
its own amplitude, frequency, phase and direction. The direction is deter-
mined by the phase difference between the control signals of the subsequent
boards for the particular component.

The components can either be put in separately or they can be calculated
from a (discretized) variance density distribution (spectrum). Also the
standard Pierson-Moskovitz and JONSWAP shaped spectra can be generated. For
each of the eighty paddles a control value is calculated 20 times per
second, taking into account the transfer function of the generator and the
wave basin. Comparison of the desired and the realized spectrum can lead to
small adjustments of the input. The wave machine is able to generate wave
directions ranging from -90° to +90°, the phase range is [-180°, +180°].

Experimental procedure.

The experimental procedure was the same for the three bottom configurations. The following steps could be distinguished.

1 The wave gauges and wave direction meters were placed in the right location.

2. The wave height part of all instruments was calibrated by changing the water level.

3. The water level was adjusted to 40.00 cm.

4. The instrument output was adjusted to zero.

5. The new calibration figures were stored in the computer.

6. The control signal for the wave generator was arranged.

7. The data collection on the computer was started about 10 minutes after the start of the wave generator.

8. After 21 minutes of data storage the wave generator was stopped and the first processing of the data took place.

9. The instrument output was adjusted to zero after the water had calmed down.

10. The next control signal for the wave generator was set up.

All eight cases of input wave conditions were performed according to steps 7 - 10. After completion of the eight cases the position of the measuring instruments was changed and above steps from step 1 on were performed for the two remaining set-ups of instruments.

After checking the first results of the data processing, the decision was made to build in the next bottom geometry.

2.6 Data collection and processing.

In this section the data collection and the data processing are briefly described. The data processing is divided in three parts: 1) the wave height data, 2) the wave direction processing and 3) special parameter evaluation for the verification of HISWA.

2.6.1 Data collection.

The wave gauge and wave direction meter signals were collected by an on-line computer digitizing the signals at 25 Hz sampling frequency. The signals were digitized during about 21 minutes, such that 32768 data points resulted (8*4096 data points).

Only a fixed set of levels was available for approximating the continuous data. In the present case the full scale of the input between -10 and +10 V was divided into 4096 equally spaced levels. The magnitude of each data point is approximated by the level closest to it and is expressed in a certain number of digits. The resulting number is multiplied by a conversion factor in order to achieve a result in engineering units which forms the basis for the analysis.

2.6.2 Standard wave processing.

The variance spectrum $E(f)$ has been calculated using each fourth data point, sothat the Nyquist frequency is 3.125 Hz. The spectrum has been calculated with partial series of 256 points, sothat the equivalent degrees of freedom for each spectral estimate is about 64. Three examples of spectra at different locations for one bottom geometry are given in Figures 6-8. Parameters which follow from the spectral calculations are the total variance, m0, the peak frequency, fm, and the peak period defined as $Tp = 1/fm$.

Also a statistical analysis has been carried out. Here zero-crossing waves are considered and the 25 Hz series are used. The parameters which are calculated are the significant wave height, <Hz,1/3>, and the mean zero-crossing wave period, <Tz>. Furthermore the 1 % wave height, Hz,1/100, has been calculated; this measure has not been used in the verification study. Other parameters which have been calculated are the maximum crest and maximum

trough amplitude and the shift of average level; also the dominant frequency fd, defined by the centre of gravity of E(f) above the line 0.8*E(fm) has been calculated; it is seen later that the difference between fd and fm is minimal. As the corresponding measure of the average wave period as used in HISWA, the wave period Tm-10, does not belong to standard data processing techniques, this parameter has been evaluated for the sites where the directional wave instrument has been stationed.

2.6.3 Wave direction processing.

From the wave height signal and the two orthogonal horizontal velocity signals information concerning the wave direction and directional spreading can be obtained. From the signals of the instrument used the distribution of the wave directions per frequency can be obtained. Here we reduce the information to one principal wave direction per frequency and one measure for directional spread for each frequency. As in the variance spectrum the Nyquist frequency of 3.125 Hz is used, the frequency range is subdivided in 128 intervals of length df = 0.0244 Hz.

From a calculation of the auto- and cross-spectra the Fourier coefficients a(f) and b(f) can be calculated and $D(\theta;f)$ can be written in terms of the zeroth and the first two Fourier coefficients, see Appendix F, section F.2. The pricipal wave direction θ_o follows then from

$$\theta_o = \arctan[b_1(f)/a_1(f)] \ ,$$

and one of the spreading measures is then (see Eq. (F.6))

$$\sigma_o = \sqrt{2\{1 - \pi[a_1^2(f) + b_1^2(f)]\}} \ .$$

The directional spreading measures are discussed in Appendix F.

2.6.4 Special data processing.

For the purpose of verification of the characteristic wave period measures as used in HISWA, also the socalled "minus 1 spectral moment", m-1, has to be calculated. For the verification of the wave periods predicted with HISWA, the variance spectra at the sites where the wave directional meters have been stationed, have been used for determination of the spectral

moments m-1, m0, m1 and m2 and different vave period measures have been calculated. As at site 10 the experiment has been repeated tvice (measurement positions 20 and 30 are at the same location), the spectra at sites 20 and 30 have also been considered.

The moments are defined as

$$m_j = \int_0^{3.125} f^j E(f) \, df, \qquad j = -1, 0, 1, 2$$

The spectral mean frequencies fm-10, fm01 and fm02 are defined as :

fm-10 = m0/m-1

fm01 = m1/m0

fm02 = $\sqrt{m2/m0}$.

Results of these spectral mean frequencies fm-10, fm01, fm02, together with the peak frequency fm are given in Appendix S. For one situation the results are discussed in section 2.7.

2.7 Spectra and vave parameters.

Some of the variance spectra E(f) as resulting from the measurements are discussed in this section. Some spectra as resulting from the measurement me35 (semi-cylindrical bar and input condition case 5) have already been shown in Figures 6-8; these spectra are in the form as resulting from the standard vave processing. In order to be able to compare the spectra with theoretical JONSWAP spectra, the spectra are normalized vith the peak frequency, fm, and the peak of the spectrum, E(fm). In Figures 9-11 the same spectra are given in normalized form together with the theoretical JONSWAP spectrum with peak enhancement factor γ_0 = 3.3. It is clearly seen that, while near the wave board, at site 10, the spectrum is of the required JONSWAP-type, behind the bar a second peak in the spectrum is present, while the first part of the spectrum remains of JONSWAP-type form. It is clear that for such double-peaked spectra one characteristic vave period is difficult to apply. Notice that the second peak is not alvays a harmonic of the peak frequency.

In order to obtain an idea of the energy content in the second peak of the

spectrum, the variance above a fixed frequency is calculated for the spec-
tra at the seven sites for each measurement condition and the three bottom
configurations. On visual inspection of the spectra, the frequency between
the two peaks in the spectra was seen to be about 1.1 Hz. The variance in
the second part of the spectrum is denoted by m0d2, while the total
variance is m0, and is defined as :

$$m0d2 = \int_{1.1}^{3.125} E(f)\, df , \qquad m0 = \int_{0}^{3.125} E(f)\, df$$

In the Table below, values of m0d2/m0 in % are given for the measurements
me35, me25 and me15, for respectively the semi-cylindrical bar, the cylin-
drical bar and the empty basin. It is seen that up to 20 % of the variance
is present in the tail of a JONSWAP-type spectrum with γ_0 = 3.3 above f/fm
= 1.1/0.8 = 1.4. Behind the bar the ratio increases up to 60 %. For the
theoretical JONSWAP spectrum we obtain for f/fm > 1.36 from Eq. (G.14) and
Table G.2 : m0d2/m0 = 19.9 %, while for the Zitman spectrum is obtained
from Eq. (G.31) and Table G.5 for the same peak-enhancement factor 3.3,
m0d2/m0 = 22.5 %. (The Zitman spectrum is defined in appendix G.)

	site	semi-cyl. me35	fully cyl. me25	empty basin me15
in front	19	20.8	19.9	18.5
of	10	20.0	18.5	17.7
bar	18	21.2	20.8	20.5
on bar	38	21.2	20.8	20.5
behind	39	37.1	51.5	17.6
bar	29	43.1	52.1	18.3
	28	60.9	51.0	17.8

Table 2.4 Values m0d2/m0 in % for case 5.

Values m0d2/m0 are given in Appendix S for all measurements mexy. Notice
that the values for the empty basin give some indication of the variability
of the wave field. Another measure on the variability is provided by the

standard deviation s(HmO) over the 26 sites as is given in Table C.99 in Appendix C. Normalizing s(HmO) with <HmO>, Table C.99 shows that for the empty wave basin measurements a variability of about 4 % in the wave heights is present, except for measurements me16 and me17, where the variability is about 10 %.

2.8 Method of verification and statistical parameters.

Boundary conditions and computations.

Computations have been performed for all cases of Table 2.3 for both the semi-cylindrical bar and the cylindrical bar configuration. The boundary conditions used as input for the numerical model have been determined from the corresponding measurements. For the wave height H the measured wave height HmO at site 10 has been taken and for the wave period as used in HISWA the measured value Tm-10 at site 10 has been used. It is noted that along the wave board the wave heights are not constant as can be seen from, e.g., Tables C.63 - C.65, which are also given below as Tables 2.5 - 2.7. In all cases the value for HmO at site 19 is highest and the one at site 18 is lowest. For the semi-cylindrical bar configuration this can be attributed to the wave-induced current which is present in the wave basin. As in HISWA only one constant wave height can be given on the start line of the computational region, the measured variability in HmO gives some discrepancies upon comparison of computed and measured wave heights; however, these errors are rather minor.

9.82		10.47		10.14	10.05
		9.78		9.28	9.79
		9.91	9.95	9.70	9.69
10.46	9.78	10.19		9.92	9.75
		10.16		10.15	9.56
10.09		9.96		10.00	9.98
11.57				9.99	10.26

Table 2.5. HmO empty basin, case 5, me15.

4.74		4.73		4.64	4.82
		4.82		4.49	4.83
		4.96	4.80	4.73	4.89
5.68	5.70	5.70		5.59	5.57
		10.07		9.96	9.25
10.18		9.98		10.05	9.86
10.93				10.23	10.03

Table 2.6. HmO cylindrical bar, case 5, me25.

11.35		7.96		6.98	6.26
		8.22		7.60	6.18
		8.31	8.07	7.38	6.29
11.28	9.93	8.74		6.14	6.25
		9.83		9.78	8.87
10.11		10.75		10.47	10.36
11.08				10.42	10.04

Table 2.7. HmO semi-cylindrical bar, case 5, me35.

As the computed wave height behind the bar depends critically on the wave breaking parameter γ, the value of γ has been determined according to the algorithm given by Battjes and Stive (1985), where for the wave period has been taken the measured value of Tm-10 at site 10. In Table 2.8 below, all values for γ for the computations ve21-ve28 and ve31-ve38 have been given. Also, for comparison only, the values γ_p as would have been obtained for the case that the peak period Tp was used are given. It is noted that the difference in computed value for the two wave period measures is very slight and is hardly significant, taken the gross estimate of γ into account. For other projects the difference in wave breaking parameter as resulting from Tm-10 can be significantly higher than the one resulting from Tp. In appendix U is shown that the present choice of γ is a good one in order to obtain equivalent effect on the wave height from the wave dissipation. Furthermore, it has to be mentioned that for the steepness parameter γ_s in the maximal allowable wave height Hm has always been taken 0.88 in the computations reported in this study (see also appendix U).

We took the values calculated with Tm-10, correct in more figures than would be relevant, in order to not introduce any deviation of computed wave heights beforehand, sothat the comparison is as fair as would be possible. Moreover, it has to be stressed that for the verification computations no validation by variation of physical model parameters has been carried out.

Because the sidewards boundaries in HISWA were dissipative (reflecting boundaries were not possible), the wave field close to these boundaries is distorted. A region with an apex of 20° starting from the start line of the computational region is considered to be the whole of the disturbed area. Tests with a horizontal bottom showed that this is rather accurate. The computational area is taken 50 m wide, whereas the lateral extension of the physical wave basin is only 26.40 m.

case	HmO	Tm-10	γ	Tp	γ_p
21	5.14	1.211	0.7071	1.241	0.6991
22	9.96	1.221	0.8192	1.241	0.8141
23	10.34	1.205	0.8290	1.241	0.8201
24	10.12	1.148	0.8395	1.170	0.8343
25	10.23	1.183	0.8328	1.241	0.8184
26	10.30	1.206	0.8282	1.254	0.8162
27	10.53	1.174	0.8391	1.217	0.8288
28	9.83	1.466	0.7523	1.254	0.8085
31	5.07	1.218	0.7030	1.254	0.6935
32	10.06	1.213	0.8228	1.241	0.8157
33	10.44	1.198	0.8322	1.241	0.8216
34	10.06	1.142	0.8401	1.159	0.8361
35	10.42	1.170	0.8385	1.241	0.8213
36	10.50	1.218	0.8282	1.241	0.8225
37	10.56	1.178	0.8385	1.280	0.8136
38	9.93	1.332	0.7895	1.280	0.8034

Table 2.8 Values of the wave breaking parameter γ.

The computational mesh.

The width of the sector in which the computation proceeds has been taken as 120°, in accordance with recommendations given in the user manual of HISWA. The computations are performed with 24 intervals for θ, so that $d\theta = 5°$. As the smallest width of the directional distribution close to the wave board is 12.5°, the value of 5° is the maximum value which might be taken. The most important condition is given by the proposed formula :

$$dx/d\theta < 0.7 \cdot |h/\nabla h| .$$

An upper value for $d\theta$ is set by the choice of the $\cos^m\theta$ distribution on the start line. For $m = 20$ one has $s(\theta) = 12.5°$ and for $m = 4$ one has $s(\theta) = 25.5°$. The most critical condition is reached for the depth $h = 0.10$ m and on the slope on the backside of the bar, where $\nabla h = 0.10$. One then has $dx/d\theta < pd$ and for pd the recommended value is 0.7; then we have $dx < 0.7 \cdot d\theta$. For dy the following condition is recommended :

$$dx/dy < 0.7/\tan(\alpha/2) ,$$

where $\alpha = 120°$ is the angle of the sector considered. With $pd = 0.7$ one obtains $dx/dy < 0.40$. Summarizing, for the present situation we have :

$$dx/d\theta < 0.70$$
$$dx/dy < 0.40 .$$

With $d\theta = 5°$ (equals 0.087 radians) there results $dx < 6.11$ cm and $dy > 15.3$ cm. As these values are very small, the values $dx = 0.10$ m and $dy = 1$ m have been used in the verification computations. It is remarked that in initial computations there was started with $dx = 0.50$ m and later also with $dx = .25$ m; for these values of dx error messages appeared with warning "negative wave action found" and also "so many c_θ-reductions present"; the latter warning concerns the presence of wave paths which turn backwards and the wave direction used in the program is altered then. A further reduction to 12.5 and 10 cm for the dx had as effect that all warnings disappeared. Because the present computations are verification computations the policy was followed that no unwanted errors were to be allowed, although the severity might be low. However, it is not clear how to measure the severity of the errors other than counting the number.

The extent of the computational region was taken 30 m in x-direction and 50 m in y-direction.

Method of comparison.

Parameters from the computations to be compared with measured parameters are the wave height H, the wave period T, the wave direction θ_o and the directional spread $s(\theta)$. The corresponding measured quantities are HmO, Tm-10, θ_o and σ_o. The wave heights are available on 26 sites, whereas the other three parameters are only available on 7 sites, the sites on which the directional meter had been stationed. The value Tm-10 could have been computed from the spectra E(f), in principle available on all 26 sites, but this was considered to be a too costly operation, especially because these spectra as such were not stored, but only the wave registrations are kept.

A direct comparison of computed and measured wave heights is given in the form of a scatter plot, which gives visual information on the corresponden-ce. In order to have some more objective measure of the correspondence, a number of statistical parameters are calculated. To that end the approach of Willmott (1981, 1984) was adopted, in which a set of statistical measu-res is adopted; this set is complete in itself, sothat also other parame-ters such as bias or correlation coefficients can be calculated from the parameters given. A description of Willmott's method is given in Appendix E. Here we consider especially the statistical parameters :

mae   the mean absolute error;

rmse   the root mean square error;

rmses   the systematic part of the rms error;

a and b   the parameters obtained from an ordinary least square regression
           between the computed and the measured values, with b the slope.

d   the index of agreement as given by Willmott, with d=1 perfect
           agreement and d=0 the case of no agreement at all.

dl   the modified index of agreement, which is more suited for cases
          near perfect agreement.

It is to be stressed that the whole of the set parameters is to be consi-
dered, as a single parameter is in most cases not suited for studying model
performance. It is noted that the parameters are not scaled, apart from d
and dl. See further Appendix E.

For all wave parameters mentioned the following procedure was follwed; as
an example it is elaborated for the wave height.

For a comparison of the computed and the measured wave height field, the
wave heights at the 26 sites are compared. From the computed wave field the
wave height at the location of the measuring position has been generated.
Furthermore, in order to have some idea of the variability of the computed
wave field over some region of space, also in a number of points around the
location of the site in question the wave heights are generated from the
computed wave field. In fact, from the computations, output is generated in
a square of 50 by 50 cm with midpoint the site in question, where 25 wave
heights are given (see the sketch below). For the comparison the mean value
over the central 9 points is used; the standard deviations are also
computed, but these are so low that equally well the central value for H
could have been taken.

```
x   x   x   x   x

x   x   x   x   x

x   x   o   x   x

x   x   x   x   x

x   x   x   x   x
```

        Sketch 2.1

2.9 Current measurements.

For the measurement conditions me35 and me38 also horizontal current mea-
surements in a grid of 3 by 3 m have been carried out. The currents are
measured in 81 points as depicted in Fig. 12 and the two horizontal compo-
nents of the GRSM have been measured at half the local waterdepth. These

measurements have been performed separately from the the wave measurements, but the same control signal for the wave board as used in me35 and me38 has been used. The measurements have been performed with the three GRSM's, so that the experiment had to be repeated 26 times to cover all measuring positions. Two wave height gauges at fixed places have been used (see Fig. 12).

At three positions the current has been measured at five depths : at 1, 5, 10, 20 and 30 cm above the bottom, see Figure 12.

At the toe of the wave damping talus the mean water level has been measured at ten different positions by means of a narrow connection and a gauge-glass.

Experimental procedure.

In the experimental procedure the following steps could be distinguished.

1. The instruments were placed at the right location and in the right direction.

2. The wave height part of all instruments was calibrated by changing the water level.

3 The water level was adjusted to 40.0 cm.

4. The calibration figures were stored in the computer.

5. The control signal of the wave generator was arranged.

6. The wave fields were given 30 minutes to develop a stable situation.

7. Ten minutes data collection.

8. The wave direction meters (GRSM's) were placed in the new position and in the right direction (the wave generator still running).

9. After the first data processing, the next data collection was started.

The last two steps were repeated till all measuring positions had been covered.

After conclusion of the measurements at all half water depth positions, the three positions were taken to measure the velocities at five water depths.

The same procedure was used for the current measurements for the measurement condition me38.

3. Confrontation of HISWA computations with measurements.

3.1 Introduction.

In this chapter the measurements of the semi-cylindrical bar geometry are used to test the performance of the wave propagation program HISWA. For all measuring conditions corresponding computations have been performed. As described in section 2.8, the comparison of the wave parameters is done for those measuring positions where the corresponding wave parameters have been measured. We consider the wave height, H, the wave period, T, the principal wave direction, θ_o, and the directional spread parameter, σ. To account for some variability, in the computations the parameters are generated in a block of sides .5 m, with the measuring position in the middle; 25 output points are taken and the parameters considered are the mean values over the central 9 points, see sketch 2.1 on page 24. Therefore the wave parameters are averaged over a region of space of 25 by 25 cm, or only over about 1/8 to 1/4 wave length.

The case of the fully cylindrical bar has also been considered, in order to have some additional information on the performance of HISWA in a simpler situation. It will be argued furtheron that this bottom geometry gives especially information on the performance of the wave period prediction.

The initial conditions for the computations are described in section 3.2, in addition to the discussion already given in section 2.8. An overview of all HISWA computations which are performed for the verification study is given in section 3.3, together with the most important wave- and computational parameters.
In section 3.4 the results of the computations are discussed, where for each of the verified wave parameters a separate subsection is given. For the wave height, both a visual presentation and one in the form of a set of statistical parameters is given, and in section 3.5 the general discussion follows.

3.2 Determination of the initial conditions.

The computational mesh of the HISWA computations has its start line at the wave board in rest; see appendix B for the position of the various meshes. As wave height H at the start line is taken the value HmO at site 10 as ob-

tained from the corresponding measurement; this value HmO is the mean of the three values at sites 10, 20 and 30, which have the same position in the wave basin. Measured values at site 10 are always the mean over the values from the repeated experiments, unless otherwise indicated. It is noted that site 10 is situated 2 m from the wave board, see, e.g., Table 2.1. This is considered to be close enough to the wave board to be able to use the measured values as input condition for the computations, although they are started at the wave board position. It is noted that the measured values HmO at 2 m from the wave board (sites 19, 10 and 18) show some variability, as is shown for example in Tables 2.5 to 2.7 for measuring condition 5, but as site 10 is situated in front of the midposition of the wave board, and only a single constant wave height H can be given as input to HISWA on the start line of the computational mesh, it was decided to take the measured value at site 10 for all computations. Likewise, for the wave period T, the value Tm-10 as resulting from the measurements at site 10 is taken as input.

The input parameter for the directional spreading parameter, σ, is the exponent of the $\cos^m\theta$ distribution. As input for HISWA are taken the values for m as given in the measuring program as given in Table 2.3. For case 8, where no directional spreading was used in the experiments, the value m = 64 has been taken, as was done by Booij et al. (1984) in a similar situation. Notice that it is obligatory in HISWA to have some directional spreading.

The spectral spread as obtained from the measurements has not been taken as input for HISWA as it is determined in a different way as discussed in appendix F, and its determination is rather sensitive to small errors in the measured velocities.

The principal wave directions θ_o have been taken to be zero for the cases 1-5 and 8, while the measured values of θ_o obtained at site 10 have been taken for cases 6 and 7 (the cases of obliquely incoming waves).

The value of the wave breaking parameter γ has been determined for the HISWA computations by appying the formula of Battjes and Stive (1985) where for the wave period the value Tm-10 instead of the peak period Tp has been used. The resulting values for γ have been given in Table 2.8.

The computations are performed with influence of bottom friction; the parameter fv has been set equal to the standard value of 0.01 in all computations. As in the wave basin the floor is of smooth concrete and the Nikuradse roughness parameter kN can be estimated as kN = 0.5 mm, the parameter fv could be estimated as fv = 0.017 to 0.058, following Jonsson (1978, 1980); notice that the laminar boundary regime is valid here. For the values of the measurement me25 along line f) the following results are obtained. Here a is the particle excursion at the bottom, ub is the amplitude of the bottom velocity (according to linear theory), Re is the Reynolds number, Re = a*ub/ν, ν is the kinematic viscosity taken to be equal to 10^{-6} and δ is the bottom boundary layer thickness; the usual mks units are used in Table 3.1. As the critical Reynolds number is equal to 30853, below which value the laminar regime holds, here the bottom friction parameter fv is evaluated according to the laminar case formula as fvL = $2/\sqrt{Re}$. Given the value of Re, the friction coefficient can be read off from the Figure as given in Kostense et al. (1986).

T	h	Hs	a	ub	Re	fvL	δ/kN
1.24	0.40	0.100	0.0318	0.161	0.511E+04	0.0280	1.62
1.24	0.40	0.099	0.0312	0.158	0.494E+04	0.0285	1.60
1.24	0.20	0.093	0.0527	0.267	0.141E+05	0.0169	2.37
1.24	0.10	0.056	0.0497	0.252	0.125E+05	0.0179	2.27
1.24	0.30	0.049	0.0203	0.103	0.209E+04	0.0438	1.16
1.24	0.40	0.048	0.0153	0.078	0.119E+04	0.0581	0.94

Table 3.1 Bottom friction parameter fvL, laminar regime (kN = .0005 m).

It is thus clear from the values fvL as given in above Table for a realistic situation for our computations that the value fv = 0.01, as used in the computations is a rather low value and is at least not too large.

3.3 Overview of the computations and the choice of computational parameters.

The computational mesh was for all HISWA computations taken as :

- dx = .10 m.

- dy = 1.0 m.

- α = 120°, where α is the apex of the sector in θ in which the computation proceeds.

- dθ = 7.5° or 5°, depending on the width of the directional distribution; for m = 20 there is taken dθ = 5° and for m = 4 there is taken dθ = 7.5°. Only for ve28 and ve38 is taken dθ = 2.5°.

The HISWA computations are denoted by ve2x for the fully cylindrical bar geometry, where x denotes the measuring condition and by ve3x for the semi-cylindrical bar geometry. In some situations a letter is added to denote a variation, such as ve35b denotes a variation on ve35, in this case the breaking parameter has been changed. The various HISWA computations are given in Table 3.2 below, together with the main parameters.

case	HmO	T	m	γ	θ_o	comment
ve21a	5.14	1.211	20	0.7071	0	
ve22	9.60	1.221	20	0.8192	0	
ve22a	9.96	1.221	20	0.8192	0	
ve23	10.34	1.205	4	0.8290	0	
ve24	10.12	1.148	4	0.8395	0	
ve25	10.23	1.183	4	0.83	0	
ve25a	10.42	1.17	4	0.80	0	Comor points
ve26	10.30	1.206	20	0.8282	28.7	
ve27	10.53	1.174	4	0.8391	29.4	
ve28	9.83	1.466	64	0.7523	0	
ve31	5.07	1.218	20	0.7030	0	
ve32	10.06	1.213	20	0.823	0	
ve33	10.40	1.198	4	0.83	0	
ve34	10.06	1.142	4	0.8401	0	
ve35	10.42	1.17	4	0.80	0	
ve35aa	10.42	1.17	4	0.84	0	ODYSSEE
ve35b	10.42	1.17	4	0.84	0	WAQUA
ve35bs	10.42	1.17	4	0.84	0	with current
ve35s1	10.42	1.17	4	0.84	0	with current s1
ve35s2	10.42	1.17	4	0.84	0	with current s2
ve35c	10.42	1.17	4	0.92	0	
ve36	10.50	1.218	20	0.8282	24.7	
ve37	10.56	1.178	4	0.8385	23.48	
ve38	9.93	1.332	64	0.7895	0	

Table 3.2 Overview of the HISWA computations.

Comments on the various computations.

ve21a   The standard case, job ve21 went wrong;

ve22   The wave height was given wrongly,
ve22a   The standard computation;

ve25   The standard computation;

ve25a   a computation performed with output for the current model, but
         with the same input parameters as ve25 in order for an intercompa-
         rison between the two bottom geometries; this case is not analyzed
         here.

ve35   the wave breaking parameter γ was too low (0.80 instead of 0.84);
         a computation ve35a has also been performed with the same input
         parameters, but with output for the current model ODYSSEE.

ve35aa   same input parameters as ve35b, but with extra output for current
         models; moreover, the averaging block has dimension of 3 by 3 m
         instead of .5 by .5 m. The values <H> used are averages over the
         central nine points, and are thus averaged over 1.5 by 1.5 m.

ve35b   the standard computation; output has been generated for the
         current model WAQUA.

ve35bs   as ve35b, but now with current refraction, where the current field
         has been determined by WAQUA in the physical basin (width 26.4 m);
         by extending this wave field sidewards for the computational frame
         of 50 m width, the HISWA computation has been performed.

ve35s1   the measured current field has been taken as input for current
         refraction; outside the physical basin domain the current field
         has been set equal to zero.

ve35s2   the measured current field has been taken as input for current
         refraction; outside the physical basin domain the current field
         has been extended as in ve35bs to fill the computational domain.

ve35c   the wave breaking parameter γ has been set to a higher value (0.92 instead of 0.84); to be compared with case ve35b.

3.4 Results of the computations.

3.4.1 Introduction.

The discussion on the performance of the computations with regard to the measurements is split up according to the different wave parameters to be compared. In first instance we focus on the prediction of the wave height, for which case most measured data is available. This is done in section 3.4.2. Next the wave period, the principal wave direction and the directional spread are considered, in sections 3.4.3 to 3.4.5 respectively. The latter three wave parameters have only been measured (or evaluated) in seven points in the wave basin.

The comparison of the computed and measured wave parameters is carried out at the one hand on a point by point basis, and secondly, measures taken over all available sites have been considered. For the point by point comparison the relative difference has been considered for the wave height and the wave period, while for the wave direction and directional spread only the absolute deviation has been considered, because, for the directions, a relative measure is senseless.

In evaluating the performance of the predictions made by the computer program HISWA, most weight has been given to the set of statistical parameters as described in section 2.8 and in appendix E. As a large number of computations have been carried out (see Table 3.2), not all results are discussed in detail, although of all computations all information at the 26 sites has been included in the report.

The wave heights at the 26 measuring sites have been given in appendix H for all computations. Also the wave periods, the principal wave directions, and the spectral spread as resulting at the 26 sites have been reported in apendices J, K and L respectively. The wave heights and the wave directions as resulting from the CREDIZ computations have also been included in appendices H and K; notice that in CREDIZ the wave period is constant and no directional spread is computed in that model.

A direct, point by point, comparison is given in appendix M for the wave height in terms of the relative deviation. For the wave periods the computed and measured wave periods have been given together with the relative deviation in appendix N, while for the wave direction and the directional spread the measured and computed values together with their absolute deviation have been reported in appendices P and Q.

The statistical parameters for the four wave parameters have been reported in appendix E for all computations.

3.4.2 Wave height.

Based on the measured values HmO as given in appendix C and the computed wave heights <H> as given in appendix H, scatter plots have been given for all cases as denoted in the overview, Table 3.2, in Figures 13 to 35. In these scatter plots, based on all 26 sites, the line of perfect agreement has been given also. These scatter plots consitute a means for visual inspection of the performance of wave height prediction of HISWA in the whole of the wave basin.

Inspection of Figures 13-21 for ve2x shows that two groups of points can be discerned, one for higher and one for lower wave heights, respectively in front of and on and behind the bar. Figures 19 and 20, for the cases ve26 and ve27, in which obliquely starting waves are considered, show a larger variability in the measured wave heights HmO than in the computed wave heights <H>. In Fig. 19, the largest values HmO are obtained at sites 19 and 16, and in the lower group the largest HmO is obtained at site 17. These sites lie close to the leftern boundary and the influence of reflection in the measurements against the perpendicular concrete walls is clearly shown in the wave height values at these sites. Notice that the same is also seen for the cases me36 and me37, although to a lesser degree because of refraction around the head of the bar, see Figs. 32 and 33.

The statistical parameters, especially suited for model performance evaluation, as discussed before, have been given in Tables E.1 and E.2 for the primary and secondary statistical parameters. It is noted that all secondary parameters can be calculated from the given values of the primary ones; tables with secondary parameters have been included for ease of the discussion. Notice that the values of these secondary parameters have been obtained from not rounded figures.

results of ve2x versus ve3x.

Focussing for the moment at the index of agreement, d, a quick glance at Table E.1 shows that the computations for the fully cylindrical bar geometry (computations ve2x) perform better than the computations ve3x for the semi-cylindrical bar geometry. This better performance of ve2x compared to ve3x is also clear from the deviation measures mae and rmse, see, e.g., Table E.2 where the relative measures have been given; for normal incidence (that is, cases ve26 and ve27 are excluded), the rms deviation is up to 5 % for ve2x, while it is around 10 % for ve3x. That the computations ve2x perform better than the computations ve3x is quite natural because of the much more simple bottom geometry. Furthermore, it has been noted previously, see, e.g., Dingemans (1985), that the modeling of wave dissipation due to wave breaking by means of the Battjes and Janssen approach is rather successful in a large variety of situations; the only problem is the choice of the wave breaking parameter γ.

Influence of choice of wave breaking parameter γ.

As the bias is predominantly (slightly) negative, while the bottom friction coefficient fw should in fact have been chosen larger, sothat a larger negative bias would have been obtained, this points to the fact that the wave breaking parameter γ should have been chosen somewhat larger. For the choice of γ we used the formula as given by Battjes and Stive (1985); however, this formula has been derived for situations where the wave period is constant in the whole of the computational region. For the fully cylindrical bar situation no variation in γ has been included in the various computations belonging to the same measurements, as it is in the semi-cylindrical bar situation (ve35b versus ve35c). As the wave-induced current is shown to be very important in the semi-cylindrical bar geometry lateron, but not so much in the fully cylindrical bar situation, a comparison of ve35b with ve35c shows only a trend, but is not conclusive in answering the needed change in the value of γ. A simple tool for studying the sensitivity of the resulting wave heights for a change in wave breaking parameter γ is provided by the one-dimensional wave propagation program ENDEC (for a description, see Stive and Dingemans, 1984), which can be applied for the fully cylindrical bar geometry for the narrow directional distribution as provided in measurement me22.

Such a study has been performed, where also differences in bottom friction
formulations have been considered, foremost variable fv versus constant fv.
As only a simple formulation for frequency change has been applied in ENDEC
for this purpose, different from the one used in HISWA, the results are not
totally comparable. Furthermore, apart from different wave breaking inten-
sity due to various fv-formulations, giving different dissipation, also
wave period change has a direct influence on the wave breaking intensity
due to the fact that the maximum wave height Hm is different due to a dif-
ferent value of the wave number k. A full discussion will be given
elsewhere; it seems that an increase of γ of 0.1 corresponding to its nor-
mal value (fixed wave period and fixed value of fv) gives about the same
result as in the case that both fv and T are variable. This conclusion is
to be taken only as some guidance, it needs not to be correct in all cases.
Further details are foreseen in another study.

The cylindrical bar geometry.

The results of computations ve21a, ve22a, ve23, ve24, ve25 and ve28, all
standard computations for the respective input conditions, can be summa-
rized as follows for the wave height. The cases for obliquely incident
waves, cases ve26 and ve27, are discussed separately.

Consider the 17 sites on and behind the bar. The statistical parameters
have been given in Tables E.7 and E.8. Values of some of these parameters
are collected in Table 3.3 below for convenience. We consider at first case
ve22a in some detail; in this case both the frequency spectrum and the
directional distribution were narrow. Next we consider ve28 in detail.

case	n	bias %	mae %	rmse %	a cm	b	d	d1	r2
ve21a	17	-0.92	2.69	3.70	0.40	0.90	0.96	0.84	0.87
ve22a	17	0.24	2.60	3.16	0.31	0.95	1.00	0.95	0.99
ve23	17	-0.82	3.61	4.21	0.31	0.94	1.00	0.93	0.99
ve24	17	-0.59	3.58	4.38	0.06	0.98	0.99	0.92	0.98
ve25	17	-1.33	3.78	4.54	0.12	0.97	0.99	0.92	0.98
ve26	17	0.12	6.34	7.57	0.01	1.00	0.98	0.86	0.94
ve27	17	-3.97	6.57	7.58	-0.22	1.00	0.98	0.86	0.95
ve28	17	0.29	5.10	6.21	-0.69	1.12	0.99	0.90	0.98

Table 3.3 Some results from Tables E.7 and E.8 for the standard
computations of ve2x.

- Case ve22a.

   □ The bias is practically zero (0.24 %) and mae = 2.60 %, rmse = 3.16 %.

   □ Looking in detail, the relative deviations δ as given in appendix M show that the largest value is δ = 7 % (sites 39 and 35). It is also seen that the deviations differ considerably along lines of equal depth, such as line 7) on which sites 27, 39, 29 and 28 are situated.

   □ Therefore, the computed wave heights <H> as given in appendix H are investigated next. It is seen that the computed wave heights on lines of equal depth are indeed the same, as was to be expected for this simple bottom geometry.

   □ The variation in relative deviations δ is thus due to variations in measured wave heights HmO. That this is the case can be seen from Table C.55, where the values of HmO for me22 have been given. The first thing to be noted is that at line 1), close to the wavemaker, the measured wave height HmO at site 19, close to the leftern boundary, is higher than at site 10, situated in front of the middle of the wavemaker. This is also true for the empty basin, me12, and for the semi-cylindrical bar, me32, see Tables C.54 and C.56.

   □ In first instance, some measure of the variability of the measured wave heights can be obtained from measurements in the empty basin, measurements me1x. Herefore we use the standard deviation, s(HmO) and the average, <HmO>, where all 26 sites are considered. It follows from Table C.99 that, for me12, <HmO> = 9.99 cm and s(HmO) = 0.28 cm. For the 17 sites we find from Table C.54 for me12: <HmO> = 10.03 and s(HmO) = 0.30 cm. Therefore, 3 % deviation between computed and measured wave heights may be due to variability in the measurements.

   □ For the variability in the measurements several processes can be indicated :

- not uniformly generated waves due to some very slight differences in the 80 flaps of the wavemaker;

- the occurrence of cross-waves in the basin, resulting in variable wave amplitude along the wave crests;

- reflection and other effects at the sidewards boundaries;

- deformation of the gravel beach, causing different reflection properties in the various measurement cases; it has been observed that on the gravel beach a sill is formed after some time due to wave breaking on the beach; the gravel beach has not been levelled after each of the experiments;

- the influence of wave-induced current fields in the basin; in the empty basin also current fields are to be expected, consisting of one large circulation cell with current vectors pointing in anti-clockwise, because of the Northern hemisphere;

- the necessary repeating of experiments for one measurement case.

□ Some check on the level of computed wave heights can possibly be obtained by averaging the measured values along a depth contour line. Consider therefore lines 4) and 7), situated on the bar and behind the bar respectively. It follows from Table C.55 for me22 that along line 4): $<HmO>_4$ = 5.45, $s(HmO)_4$ = 0.10 and along line 7): $<HmO>_7$ = 4.73, $s(HmO)_7$ = 0.21 cm. In the computation ve22a we have $<H>_4$ = 5.35 and $<H>_7$ = 4.85. It is thus seen that the computed wave heights at lines 4) and 7) lie just in the interval given by ($<HmO>_i$ - $s(HmO)_i$, $<HmO>_i$ + $s(HmO)_i$), with i = 4, 7. The fact that the computed wave height at line 4), at the end of the breaker zone, is lower than the (averaged) measured one can be attributed to a somewhat too low value of the wave breaking parameter γ, whereas the too high value of the computed wave height at line 7) is probably due to a too low bottom

dissipation in the computations, $fv = 0.01$ instead of about $fv = 0.05$ as is inferred in Table 3.1.

- Case ve28.

  □ In the corresponding measurement, me28, no directional spreading has been applied, but uni-directional waves have been generated.

  □ It follows from Tables E.7 and E.8 that the results of ve28 are less accurate than the results obtained from the first five cases. So is, for 17 sites, for case ve28 : mae = 5.10 %, rmse = 6.21 %, while for the first five cases mae $\leq$ 3.78 % and rmse $\leq$ 4.54 %.

  □ The Table for the relative deviations δ in appendix M yields a maximum $\delta = 12.9$ % at site 28; notice that at site 18, close to the wavemaker, $\delta = 8.9$ %.

  □ The measured values HmO have been given in Table C.73. At lines 4) and 7) is obtained: $<HmO>_4$ = 5.25, $s(HmO)_4$ = 0.16 and $<HmO>_7$ = 4.88, $s(HmO)_7$ =0.44 cm. At line 7) a variation of 9 % in wave heights is present in the experiment.

For the other standard computations with normal wave incidence, cases ve21a, ve23, ve24 and ve25, the results are about the same as obtained for case ve22a. It is noticed that from this series case ve21a, the case for low wave height, performs least in regard of the index of agreement d, the coefficient of determination, r2 and the regression parameters a and b. For the regression being less, Figure 13 shows that the (26) points are located close to each other in case of ve21a, whereas for the other cases two distinct sets of points can be discerned; for the latter case a better regression can be obtained. Notice furthermore that the value of the coefficient of determination does not depend on the regression. The other parameters such as mae and rmse do in fact show a better performance for ve21a than for the other cases (ofcourse the relative values are to be compared), while the bias for ve21a is somewhat larger than in the other cases. The relative low values for the indexes of agreement is explained in next paragraph. Here is an example of the need to consider the full set of statistical parameters together, and not base ones conclusions on a single parame-

ter. As a further means of comparing the cases, the relative deviation δ, as given in appendix M, can be considered. For the present cases the value $<|\delta|>$, taken over 17 sites, ranges from 2.75 to 3.69 %, while mae and rmse range from 2.69 to 3.78 and from 3.70 to 4.54 % respectively. These are all very low values, well under 5 %, sothat it may be concluded that these cases for the fully cylindrical bar perform very good with regard to wave height.

It is remarked that the results of <H> as presented in appendix H, show that the wave heights are not exactly equal along lines of equal depth (lines 4 to 7) for cases ve23, ve24 and ve25 as it was for case ve22a. Notice that the difference is in the larger directional spread for ve23 to ve25 (m = 4) compared to ve22a (m = 20). The difference in <H> is very small and is clearest seen at site 27. For the discussion we now focus on case ve23; the other two cases show the same behaviour. Site 27 lies rather close to the physical boundary of the wave basin; the computational sidewards dissipating boundary lies much further away. Even then site 27 lies on the border of the disturbed region, as also can be inferred from the value of the principal direction <θ> and the standard deviation, $s(\theta)$, obtained by averaging over small blocks, see appendix K; here <θ> = 1.45° instead of a value much closer to zero as obtained for the other sites. Some deviation, but less, is also seen for site 28; here the deviation is less because this site is situated further from the computational boundary. For a smaller directional spread as in ve22a the sidewards boundaries have a smaller effect at sites 27 and 28, as is reflected in the values of <θ> (0.46° and 0.36°) yielding no visible deviation in <H>.

The relatively low value for the modified index of agreement d1 for case ve21a compared to, e.g., that of ve22a, can be explained in the following way; it is stressed that the regression as such is not of importance here. Considering the expression for d1 as given in appendix E, we see that the denominator of the rate is equal to the sum of the absolute deviations between the predictions, y(i), and the measurements, x(i). The nominator consists of the potential error, $\sum [|y(i)-<x>| + |x(i)-<x>|]$. As for ve21a the pairs {x(i),y(i)} lie close to each other, the potential deviation is small (<x> lies close to all x(i) and all y(i)). For case ve22a a large variation

is obtained, which is also reflected in the standard deviations s(HmO) and s(Hc) which are about 33 % while they are about 10 % for ve21a. The potential deviation in case ve22a is then much larger than the one obtained for ve21a. As the mae in the two cases differs only a factor two (0.13 versus 0.23 cm), giving about the same relative mean absolute deviation, the value for d1 is higher for ve22a than for ve21a. We furthermore notice that near perfect agreement, the case that the potential deviation is much larger than the real deviation, the measure d1 is more sensitive than the quadratic measure d, because the ratio goes faster to zero for d than for d1. We notice furthermore that the modified index of agreement d1 is still rather large because the deviation is so small (the points in the scatter diagram are aligned close to the perfect regression line); the situation for ve31 is different, the scatter plot shows a more circular distribution of the points, see Fig. 22.

Computations ve26 and ve27, both for oblique wave incidence, perform much less in relation to the normal incidence cases. This is especially the case for the parameters mae and rmse. Also <|δ|> and also the standard deviation of |δ|, s(|δ|), are significant higher. For the less performance of the obliquely incident cases the following reasons can be discerned.

- The computations ve26 and ve27.

  □ Because of the decrease in wave period T, the principal wave directions behind the bar are 6° different from the value in front of the bar (about 22.5° versus 28.6° for ve26).

  □ The deviation of <H> at site 27 compared to the ones at sites 39 and 29 is less than in the normal incidence cases, whereas at site 28 it is slightly larger. To understand this phenomenon one should be aware of the fact that the dissipating condition at the sidewards boundaries in fact works as it should be in the case of normal incidence on that boundary. For wave propagating parallel to that boundary, the effect is some 'attraction' of energy towards the boundary, resulting in wave directions turning towards the boundary. Because for computations ve26 and ve27 the initial directions are about 25 and 29°, thus the waves are propagating towards the leftern sidewards boundary, the effect of the dissipating condition is less than in the other

computations, the deviation of normal incidence to that boundary
is less.

- The measurements.

□ The reflection in the physical wave basin can be expected to be
rather high for obliquely incident generated waves . Because the
sidewards boundaries are vertical concrete walls, the reflection
coefficient is to be expected to be near one because not much
wave dissipation is likely to occur in that situation. A compar-
ison of measurements with a reasonable amount of reflection with
computations with no reflection is therefore not a fair
comparison.

□ While at site 27 effects of reflection are expected, at site 28
the effect of a shadow zone is to be expected. This effect is
most clearly seen in the measurement me16 for the empty basin,
see Table C.66. While at sites 27, 39 and 29 the wave heights
are 11.77, 11.78 and 10.68 cm respectively, at site 28 we only
have HmO = 8.37 cm. Because me17 is the measurement with larger
directional spread, the effect of shadow working is less as is
also clear form Table C.69 (10.86, 11.14, 10.97 and 10.34 cm).

□ This shadow zone is also clear from considering HmO from the
measurements me26 and me27 as given in Tables C.67 and C.70.

The effect of the shadow zone is also reflected in the relative deviations
δ as given in appendix M. For the low directional spread in ve26 deviations
from 10.4 to 18.6 % results for sites 28, 25 and 24, while deviations of
only 4.8 to 5.7 % result for ve27 for the same sites. Notice moreover that
the computed wave heights are larger than the measured ones for these
sites, while this is reversed for most other sites. This is another indi-
cation for the effect of the shadow zone in the measurements for the fully
cylindrical bar topography.

Conclusion for ve2x.

It has already been concluded above that the correspondence between compu-
ted and measured wave heights is very satisfactory, especially for the

normal wave incidence cases. The correspondence is less for the obliquely incident cases, but this is mostly due to reflection and shadow zones for the measurements in the wave basin. As also has been discussed, this correspondence has been obtained despite a too low bottom friction coefficient and a possibly too low wave breaking parameter; as these not optimal settings yield opposing effects, but of a different nature (at least in different regions of space), it is hard to ascertain whether it is possible to obtain an even better agreement. Because with simple settings of the parameters, without optimizing, already such good results are obtained, no further computations have been carried out for this simple bottom geometry. Furthermore, the geometry of the semi-cylindrical bar was the primary geometry upon which the performance of HISWA had to be tested.

Aspects of the computations and of the measurements have been discussed in some detail. One of the reasons for this is that the simple geometry enables one to draw consistent conclusions from even very small deviations. Therefore aspects of the computations have been pointed out, while some of these aspects would not deserve a second thought for purely engineering purposes.

One should be aware of the fact that the wave height prediction is rather good, despite the fact that the wave period prediction is rather much off, see section 3.4.3.

The semi-cylindrical bar geometry.

The standard computations for the semi-cylindrical bar geometry are **ve31 - ve34, ve35b** and **ve36 - ve38**. The results of these standard computations are discussed first. In order to facilitate the discussion, the values of some parameters as reported in Tables E.7 and E.8 are given in Table 3.4 below for the standard computations.

We consider at first cases **ve31 - ve34** and **ve35b**; lateron the case without directional spread, **ve38**, and the two obliquely incident wave cases, **ve36** and **ve37**, are considered.

case	n	bias %	mae %	rmse %	pes %	a cm	b	d	d1	r2
ve31	17	-5.21	8.14	10.44	49.12	2.11	0.52	0.72	0.54	0.36
ve32	17	-5.24	7.90	9.79	28.76	-0.52	1.02	0.94	0.79	0.85
ve33	17	-8.25	9.78	11.37	60.81	-2.12	1.19	0.92	0.73	0.89
ve34	17	-7.49	9.32	10.79	67.51	-2.98	1.32	0.91	0.71	0.91
ve35b	17	-7.83	9.67	11.09	61.84	-2.42	1.23	0.92	0.72	0.90
ve36	17	-7.45	12.45	13.88	35.45	0.64	0.84	0.90	0.70	0.75
ve37	17	-12.47	15.08	16.91	55.67	-0.18	0.90	0.83	0.61	0.70
ve38	17	0.57	7.51	9.37	5.99	-0.84	1.12	0.95	0.78	0.84

Table 3.4 Some results for the wave heights from Tables E.7 and E.8
for the standard computations of ve3x.

Cases ve31 - ve34 and ve35b.

We see that the bias is between about -5 to -8 % and the mean absolute
error, mae, ranges from 8 to 10 % while the root mean square error, rmse,
ranges from 10 to 11 %.

Compared to the corresponding cases for the fully cylindrical bar, these
figures show a much less correspondence to the measurements. However, as is
to be discussed lateron in this section, we think that this is mainly due
to the generation of wave-induced currents. For the semi-cylindrical bar
the wave-induced current field (due to wave breaking) is much more compli-
cated than in the case of the fully cylindrical bar, because in the first
case, apart from a large circulation pattern, also a circulation cell
closely behind the tip of the bar is generated as measurements show. In the
fully cylindrical bar geometry at most two simple circulation patterns can
be generated, one behind the bar and (if any, then a very weak one) in
front of the bar. As in this case the current vector is predominantly or-
thogonal to the principal wave direction, not much influence of the current
on the waves is to be expected. It is remarked that the measurements are
started 10 minutes after the wave board has been started, so that it may be
safely assumed that the current distribution in the wave basin was fully
developed when the data acquisition started.

Cases ve31 and ve32.

Again the case with the low wave height, case ve31, is seen not to perform so well, especially when noting that in this case no strong wave-induced current pattern can be generated as in the other cases. For the regression being not so good and, consequently, the coefficient of determination r2 being relatively low, the same reasons can be put forward as was done before for the case ve21a. For the indexes of agreement being rather low, the same explanation can be put forward as was done in the discussion of the performance of ve21a. Remains the fact that for ve31 a better performance with respect of the bias, mae and rmse is to be expected because of the (near) absence of wave-induced currents. (Notice that this reason is not valid for ve21a.) Consider therefore the results of ve31 in more detail. The relative deviations del as given in appendix M give no significant different results from the other standard cases, as is also true for $<|\delta|>$ and $s(|\delta|)$. The variability of the measurements cannot be evaluated from measurements me31 as was the case for me21 and me11; therefore the variability of measurements me21 for the cylindrical bar and measurements me11 for the empty basin is compared to the variability of me22 and me12; the suggestion then is that the same conclusions would hold for the variability of the measurements with low wave height in the semi-cylindrical bar geometry.

As noted in the discussion of case ve22a, we have for all 26 sites from measurement me12 : $<HmO>$ = 9.99 cm and $s(HmO)$ = 0.28 cm; for the 17 sites we have $<HmO>$ = 10.03 and $s(HmO)$ = 0.30 cm. For the case me11 we have for 26 sites : $<HmO>$ = 5.15 and $s(HmO)$ = 0.16 cm, while for the 17 sites there is obtained from Table C.51 : $<HmO>$ = 5.17 and $s(HmO)$ = 0.16 cm. In both cases the variability is thus seen to be 3 %, and no significant difference between the measurements with low and high waves can be discerned. The variability in wave height along line 1) close to the wavemaker is 2.5 % for me31 and 4.5 % for me32 and, thus, this gives no reason for the relatively bad performance of ve31 in relation to that of ve32. In fact, considering all 26 sites, the values for the bias, mae and rmse given in Tables E.1 and E.2 show a slightly better performance for ve31 compared to ve32 (see below); this is due to the lesser variability of the measurements me31 in front of the bar compared to that of me32.

Considering the definitions of the indexes of agreement d and d1 as given in appendix E, and the scatter plots for ve31 and ve32, Figs. 22 and 23, we

notice the following, concentrating on d1. The mean absolute error of ve32 is about twice the one of ve31; the nominators of the expressions for d1 thus differ a factor 2. However the denominators of d1 differ much more in the two cases. The values $|y(i) - <x>|$ and $|x(i) - <x>|$ are much larger for ve32 than they are for ve31, because in ve32 a large range of values is found whereas the values are clustered near the mean value in case ve31. Therefore the large potential error for ve32 yields a small value of the fraction and thus a large value for d1. Under the supposition that the points in the scatter diagram lie uniformly distributed within a circle with its centre on the theoretical line $y = x$, the denominator is about twice the value of the nominator, yielding a value of d1 close to 0.5. In the same way there comes then d = 0.75. This estimation of order of magnitude is not too far off, for ve31 the real value for d1 is 0.50 and for d the real value is 0.72.

case	n	bias %	mae %	rmse %	a cm	b	d	d1	r2
ve31	26	-4.19	6.37	8.66	2.06	0.55	0.72	0.50	0.37
ve32	26	-4.82	6.90	9.36	0.05	0.95	0.95	0.81	0.86

Table 3.5 Some results for the wave heights from Tables E.1 and E.2
for the computations ve31 and ve32.

The relative deviations δ have been given in appendix M. For ve31 and ve32 we have for the cases of all sites (26), the sites on and behind the bar (17) and the sites on the downward slope and behind the bar (10) the following relative measures :

case	n	$<|\delta|>$ %	$s(|\delta|)$ %	bias %	mae %	rmse %
ve31	26	6.29	5.60	-4.19	6.37	8.66
ve32	26	7.13	6.02	-4.82	6.90	9.36
ve31	17	7.97	6.11	-5.21	8.14	10.44
ve32	17	8.16	5.87	-5.24	7.90	9.79
ve31	10	11.26	5.76	-9.13	11.69	13.35
ve32	10	10.16	6.59	-8.60	10.32	12.54

Table 3.6 Relative deviations in wave height for ve31 and ve32.

A detailed comparison of the performances of ve31 and ve32 shows that both
cases perform almost equally well; the performance itself is seen to depend
heavily on the region of space to be considered, the most critical region
is behind the bar. Considering the variability in wave heights for the
whole basin (26 sites) and the region behind the crest of the bar (10
sites) we have for the relative standard deviations (made relative with the
mean) the following values for me31 and me32 and for ve31 and ve32 :

n	me31	ve31	me32	ve32
26	9.13	8.70	21.13	22.70
17	11.04	10.17	19.92	23.19
10	14.23	10.07	16.53	14.44

Table 3.7 Relative standard deviation for wave height in %.

Table 3.7 shows that, for the small amplitude case, the variability in wave
heights is less for the computation than it is for the measurement. For the
higher wave height case the difference is not significant. The conclusion
is that the fact that the small wave height case, ve31, does not perform
significantly better than the large wave height case, ve32, is partly due
to the larger variability of the measurements me31. Notice moreover that
the wave directions and the wave periods are quite accurate for case ve31,
while these are not very good for ve32, see sections 3.4.3 and 3.4.4.

Case ve35b.

As depicted in Table 3.4, it is seen that cases ve33, ve34 and ve35b per-
form less than case ve32. It has to be reminded that in measurement me32 a
narrow directional distribution was used, while in me33, me34 and me35 a
wider directional distribution was used (m=20 versus m=4). One of the fea-
tures of ve33, ve34 and ve35b is that the regression is significantly less
compared to the one of ve32; the lesser performance is also reflected in a
slightly lower value of the index of agreement d. The coefficient of deter-
mination r2 shows an opposite trend, but in the light of the discussion of
Wilmott (1981, 1984), not much attention is given to this fact because r2
is not well suited for determination of model performance. One of the rea-
sons that the larger directional spread cases gives rise to less perfor-

mance could be because in that case more reflection due to the sidewards boundaries is present; some effect of this behaviour has already been noted for the measurements in the empty basin in the discussion of the performance of cases ve2x. A second reason could be the difference in generation of wave-driven currents for different directional distributions.

As the parameter pes, denoting the proportion of systematic error to the mean square error, is around 60 % for ve33, ve34 and ve35b, as given in Table E.8, it is clear that the model performance could be improved for these cases. A high value of pes indicates that either the parameter setting is not optimal, or that an effect has not been modeled. Some improvement can be obtained by choosing a somewhat higher wave breaking parameter γ, as can be seen by comparing ve35b with ve35c (γ = 0.84 versus 0.92). All parameters, except r2, show that ve35c performs better than ve35b, see Tables E.7 and E.8. Some parameters are collected in Table 3.8 below.

case	n	bias %	mae %	rmse %	pes %	a cm	b	d	d1	r2
ve35b	26	-6.56	8.13	10.45	40.85	-1.14	1.06	0.94	0.79	0.87
ve35c	26	-4.47	6.81	9.15	24.00	-0.26	0.98	0.95	0.81	0.86
ve35b	17	-7.83	9.67	11.09	61.84	-2.42	1.23	0.92	0.72	0.90
ve35c	17	-4.36	7.48	8.76	34.16	-1.61	1.16	0.94	0.77	0.88

Table 3.8 Wave height results for ve35b and ve35c.

An effect which has not been modeled in the previous computations is the effect of the wave-driven currents on the wave height distribution. The current refraction effect has been studied in the following way.

Firstly, the wave-driven current distribution has been calculated with a current program, WAQUA, by using the wave-driven forces, obtained by numerical differentiation of the radiation stresses as calculated with HISWA for the case ve35b, in the physical basin. The resulting current field has been extended to the whole of the computational domain (50 m wide instead of 26.40 m wide) and has been taken as input for the computation ve35bs. The current field has been given in the not too clear Figure 36. The results for the wave heights for ve35bs show a markedly better performance

than is obtained for the case without current refraction, ve35b. The wave
directions show that the circulation cell is not positioned at the right
place; this follows from the value for the principal wave direction at site
38.

Secondly, the wave-driven current field as has been measured in 81 points
for the measuring condition me35 has been interpolated to the bottom grid
in the physical basin. As it is not clear how to extend the current field
to the computational domain, this extension has been carried out in two
ways. In the first case the current field has been set equal to zero out-
side the physical basin; this current distribution has been denoted by s1.
In the second case the current field has been extended into the computatio-
nal domain, as was done with the WAQUA current field. A precise descrip-
tion of the procedure has been given in chapter 5. As could be expected,
use of the measured current distribution for current refraction in HISWA
yields even better results for the performance of HISWA, as can be seen in
Tables E.7 and E.8. For convenience some parameters are collected in Table
3.9 below.

case	n	bias %	mae %	rmse %	pes %	a cm	b	d	d1	r2
ve35b	17	-7.83	9.67	11.09	61.84	-2.42	1.23	0.92	0.72	0.90
ve35bs	17	-0.50	6.62	7.62	2.72	-0.58	1.07	0.95	0.79	0.85
ve35s1	17	-3.16	4.04	5.18	37.13	-0.25	1.00	0.98	0.86	0.94
ve35s2	17	-4.25	4.85	6.05	49.48	-0.19	0.98	0.97	0.83	0.93
ve35c	17	-4.36	7.48	8.76	34.16	-1.61	1.16	0.94	0.77	0.88

Table 3.9 Wave height parameters.

It is thus seen that the wave-driven current has profound influence on the
wave height distribution. This is clear from the deviations mae and rmse
and also from the regression. We considered here 17 sites, but the same
conclusions hold for all 26 sites; the same trend is seen, but with slight-
ly different values for the parameters, see Tables E.1 and E.2. The value
of pes for the cases ve35s1 and ve35s2 shows that some improvement still is
possible in the performance. Because a higher value of the wave breaking
parameter γ was seen to result in considerable improvement (ve35b versus
ve35c), it is expected that inclusion of current refraction together with a

higher value of γ yields an even better performance.

Case ve38.

Case ve38 is the case with the mean JONSWAP spectrum without directional spread in the measurements. For the computations, the exponent m of the $\cos^m\theta$ distribution has been set equal to 64. Case v38 is to be compared with ve35b in which case m = 4 has been taken; the difference in the two cases lies in the directional distributions differences. In contrast with case ve28, it is seen from Table 3.4 and from Tables E.7 and E.8 that the results for ve38 are slightly better than for the first five cases (ve31, ve32, ve33, ve34 and ve35b). Considering the computed and measured wave heights as given in appendices H and C, we notice behind the bar an essential difference between cases ve35b and ve38. At sites 39, 29 and 28 the wave heights are as given in Table 3.10 below.

case	site 39	29	28
me38	7.89	6.25	5.31
ve38	6.40	6.98	6.46
me35	7.96	6.98	6.26
ve35b	6.93	6.56	5.97
ve35s1	7.75	6.62	6.28
ve35s2	7.34	6.44	6.28

Table 3.10 Wave heights.

It is thus seen that for ve38 at site 29 the highest wave height is obtained, while the measurements show a decrease in wave heights for site 39 to site 28. In computation ve35b the trend of the measurements is followed. From the wave height it seems that site 29 is situated in a caustic region for case ve38, but the computed wave directions give no indication for this suggestion as is discussed below.

Investigating the principal wave directions as computed for ve35b and ve38 and given in appendix K, no significant difference between the two cases can be discerned other than the observation that for ve38 the directions

are about 3° larger than is the case for ve35b. From a comparison of the
measured and computed principal wave directions as given in appendix P, it
is seen that the difference in measured wave directions is especially large
at site 29, about -10° for me35 versus +2° for me38.

The results for the wave heights on he backward slope and behind the bar
show the following results for ve38 and ve35b (see Tables E.11 and E.12).

case	n	bias %	mae %	rmse %	sd %	s(Hc) %	s(HmO) %
ve35b	10	-13.01	13.01	13.99	5.42	13.50	11.61
ve38	10	-2.00	8.12	10.74	11.12	15.63	15.01

Table 3.11 Parameters for wave heights at a few sites.

Cases ve36 and ve37.

The obliquely incident cases ve36 and ve37 perform least of the standard
cases for the semi-cylindrical bar geometry. An intercomparison of the two
cases shows that ve36 (for which the two-dimensional spectrum is narrow in
both frequency and direction) performs better than case ve37 for which a
mean JONSWAP spectrum with reasonable wide directional distribution is
used. The influence of the obliquely incidence on the model performance is
seen by comparison of ve36 with ve32 and by comparing ve37 with ve35b.

case	n	bias %	mae %	rmse %	a cm	b	d	d1	r2
ve32	17	-5.24	7.90	9.79	-0.52	1.02	0.94	0.79	0.85
ve36	17	-7.45	12.45	13.88	0.64	0.84	0.90	0.70	0.75
ve37	17	-12.47	15.08	16.91	-0.18	0.90	0.83	0.61	0.70
ve35b	17	-7.83	9.67	11.09	-2.42	1.23	0.92	0.72	0.90

Table 3.12 Wave height parameters.

The results of ve36 and ve37 are consistent with those of ve32 and ve35b.
The less performance of ve36 and ve37 is believed to be, at least partly,
due to the large reflection of the waves against the side walls in the mea-
surements; therefore the obliquely incident cases are not so suited for

verification purposes. Nonetheless, the deviations between computations and measurements are not too large.

Conclusions for ve3x.

As a whole, the computations ve3x perform less than the computations ve2x. As there are generated currents due to wave breaking in the semi-cylindrical bar geometry with maximum velocities of 30 cm/s, these currents have been shown to have a profound effect on the performance of the wave prediction capabilities of HISWA, at least concerning the wave height prediction. As these currents are expected to be of much less importance in the case of the fully cylindrical bar geometry (at most one or two current cells might be expected to be generated behind the bar, not one large cell covering the whole wave basin), the effect of wave-driven currents in the computations ve2x is thought to be much less than in computations ve3x.

Without current refraction the wave height prediction is already quite good, for the standard case the modified index of agreement is dl=0.72 for the 17 sites, while for the cases with current refraction, ve35s1 and ve35s2, it is 0.86 and 0.83. Comparing ve35b with ve35s1 we see that the bias reduces from -7.8 % to -3.2 % and the for the bias corrected root mean square error, sd, reduces from 8.1 % to 4.2 %. An even better performance could have been obtained by optimizing the parameter setting; this follows from the proportion of the mean square error, which is still 37 % for ve35s1. We conjecture that a higher breaking parameter γ could do the job, as already partly indicated by the results of case ve35c in which a higher wave breaking parameter than in ve35b has been used.

3.4.3 The wave period.

The wave frequency used in HISWA is a mean frequency and therefore the corresponding mean wave period, Tm-10, has been calculated from the measured variance densities. This has been performed for the seven sites, where also wave direction information has been obtained. A direct comparison of the measured and the predicted wave periods has been given in appendix N, in which also the relative difference between the two has been given. The most suitable configuration to test the performance of the wave period prediction is given by the fully cylindrical bar geometry; that means that the

measurements me2x are especially suited for this purpose.

From the results in appendix N it is clear that on and behind the bar the predicted wave periods are rather much off from the measured ones. Except for the case of low wave height (ve21a), the computed wave periods are about 30 % too low compared to the measured ones.

The same low correspondence for ve22a, ve23 to ve38 is visible in the values of the statistical parameters as given in Tables E.33 and E.34. A bias of about -18 % and a root mean square error rmse of about 17 % are found for the cases of ve2x; notice that all seven sites have been taken into consideration here. The indexes of agreement d and d1 are up to .4 and the coefficient of determination r2 is also quite low. This low correspondence is especially significant when comparing it with the results of the wave height at the same seven sites; for the wave height H we have from Tables E.15 and E.16 a value of d of nearly 1 and rmse = 5 % and bias less than 1 %. Comparison of the other parameters for H and T shows the same trend; the performance of the prediction for the wave periods is much less than the one for the wave heights.

We note that the regression is very bad (slopes b of +3) and that even in one case, for ve28, a negative slope for the regression line is obtained; in the latter case we also have d1 > d, while usually there is d1 < d.

A reason for the rather bad prediction of the wave periods has to be sought in the way in which the wave period change has been modeled.

For the change in characteristic wave frequency a similarity approach has been followed, where the spectrum in k-space has been taken of a simple form consisting of a k^{-3} slope for k > km and zero for k < km, where km is the peak wave number. In cases of wave dissipation, the amount of dissipated energy is taken from the left side of the spectrum and the value km therefore increases and thus the frequency ω increases.

As the frequency is a function of direction in HISWA, for all directions separately the corresponding frequency is changed according to the wave dissipation in that direction and the wave action in that direction. The single wave frequency we consider,

is obtained by an integration over the directions with the wave
action as weight functions, see appendix A.

This way of modeling frequency change in the spectrum may be useful only in
the situation that the frequency spectrum remains uni-modal. It is seen
from the experiments that the spectra are here typically bi-modal. It is
believed that in all situations where considerable wave breaking occurs on
underwater bars, the variance spectrum does not remain uni-modal. Notice
that the Dutch coast is for a large part protected by longshore bars, which
can be shown to be generated by cross-shore transport mechanisms. In such
bar-typed bottom geometries, the program HISWA is expected to yield mean
wave periods which are far off from the true mean wave periods. Therefore,
HISWA can in our opinion not be used for wave period predictions in such
situations at this moment, with the present modeling of wave period change.
As found recently in another project, where a bottom geometry without bars
was present and a wave breaking zone of large extent was found for the
mildly sloping bottom, the modeled change in frequency was seen to have
profound effect on the diminuation of wave height over the breaker zone;
see also appendix U.

A difficulty in operating the program now arises. Sufficient evidence has
been given for the fact that wave period prediction is not good enough for
use in many practical situations. However, with the present modeling of the
change in mean wave period, the results of the wave height predictions have
been shown to be excellent in the present study. It has to be stressed that
in the present project no computations have been performed where the wave
period has been taken fixed, as is possible in HISWA. Thus the conclusion
that the wave period has to be taken fixed for practical situations (giving
a better performance for T in the present measurements) is not valid now,
simply because it could be that the wave height performance deteriorates
then; we have no information to decide.

For the case of the semi-cyindrical bar geometry the predicted wave period
comes much closer to the measured one because a large amount of wave energy
is not dissipated and reaches the sites behind the bar due to refraction
over the tip of the bar. This is especially true for the cases where no
current refraction due to the wave-generated current is taken into account.
When these currents are accounted for, the refraction round the tip of the
bar is less sothat less "unperturbed" wave energy is present behind the

bar. This results in predicted wave periods which are even less accurate than in the case of no current refraction (compare the results for ve35b, ve35bs, ve35s1 and ve35s2 in appendix N). Notice that both the wave height prediction and the wave direction prediction are much more accurate when current refraction is taken into account.

3.4.4 Principal wave direction.

The measured and computed principal wave directions have been given in appendix P for the seven sites where directional information has been obtained. The deviation between the two has been given in degrees. From the results it is clear that the measurements have an inaccuracy of a few degrees, up to 4°.

This becomes clear by considering the values θ_m for the sites 19, 10 and 18 in front of the wavemaker; instead of a direction close to zero there are obtained values between +4° and -4°.

In view of the inaccuracies of the measurements, the computations for the fully cylindrical bar give accurate results for the computations ve2x. It has to be noted that refraction effects for ve21 to ve25 are practical absent in this situation. It is therefore natural to base the correctness of the prediction of the principal wave directions on the case of the semi-cylindrical bar geometry. The fully cylindrical bar geometry can be used to obtain information concerning the accuracy of the HISWA computations (such as the symmetry of the results, the effect of the lateral boundaries, etc.).

For the semi-cylindrical bar the site where refraction effects are expected to be largest is site 38, situated on the tip of the bar. In fact, this location has been chosen after performing some initial computations with HISWA as the point where the change of the wave direction was largest. So for the prediction of wave direction the site 38 will take most weight in the following discussion.

Considering computation ve31, the one with the low wave height, it is seen that at site 38 the measured and computed wave direction are respectively -29° and -32°, and are thus equal for all practical purposes, also in view of the accuracy in the measurements.

For the other computations the situation is different : the measurements for me32 to me35 give about -14°, whereas the computations give about -33°. Focussing on the measurement me35, the case with the mean JONSWAP spectrum and a not so narrow directional distribution, it will be shown subsequently that the deviation of -19° for ve35 and ve35b is in fact due to the generation of a current field which is due to wave breaking.

We notice that for the refraction a slight dependence on wave height is present in HISWA; this is mainly due to the method of accounting for wave breaking :

> Compare computations ve35, ve35b and ve35c which differ in the wave breaking parameter γ, which is respectively 0.80, 0.84 and 0.92. At site 38 the computed wave directions θ_c are -33.50°, -33.10° and -32.32° respectively. Thus, the less dissipation due to wave breaking, the closer the wave direction to the one of the linear case (see ve31 for which θ_c = -32.16°).

A computation ve35a has been performed, using the same input conditions as ve35, but now also output of wave induced forces has been generated on the same grid as is used in a current model, ODYSSEE. The resulting current vectors and stream function have been given in Figures 67 and 68. It is seen by comparison with the measured current field as given in Figure 77, that the current field computed with ODYSSEE gives a rather good picture of the currents in the basin, also with nearly correct magnitudes.

A computation ve35b has been performed and the resulting driving forces have been put into another current program, WAQUA, and the resulting current field from that current computation has been used as input for the HISWA computation ve35bs to account for current refraction. For the latter case θ_c = +5.0°, and thus the same order of error in the directions occur, but now in the other direction; this is due to the fact that site 38 lies just within the wave-driven current cell which is generated closely behind the tip of the bar, as can be seen from the measured current distribution. The circulation cell as calculated with WAQUA is not in the right position.

Taking the measured current velocities as input for HISWA, the computations ve35s1 and ve35s2 have been performed, resulting in computed wave directions θ_c = -13.18° and -11.62° to be compared with the measured direction θ_m = -13.88°. The difference between cases ve35s1 and ve35s2 is solely in

accounting for the current distribution outside the physical wave basin; notice that the computational region is larger than the wave basin itself. For ve35s1 the current field outside the physical basin has been set equal to zero, while for ve35s2 the current field as obtained close to the side-wards boundaries of the wave basin has been extended to fill the whole of the computational domain.

With accounting for current refraction the wave directions at sites 29 and 28 are seen to be much closer to the measured values, but nonetheless, still deviations of 6 to 7° are present, while at site 38 the deviation is practically zero.

The difference in wave directions for the cases without and with current refraction has been shown visually in the vector plots as given in Figures 45 to 47.

The accuracy of the computed wave directions.

For testing the accuracy of the HISWA, the computations ve2x are very well suited. Because for the cases ve21a, ve22a, ve23 - ve25 and ve28 the start direction is 0°, and we have bottom contours parallel to the y-axis, the principal wave direction should equal to zero in the ideal case. Deviations from zero in θ_c are a measure for the inaccuracies of the HISWA computations as such. The results for θ_c have been given for all computations in appendix K for all sites. We first consider the directions as obtained for line e), which lies in the middle of the wave basin and is also the middle of the computational domain. We notice the following.

- For cases ve21a and ve22a, the cases with a narrow directional distribution, the directions behind the bar are 0.52° and 0.37°. For the cases with a relatively wide directional distribution, cases ve23 - ve25, the principal wave directions are at most 0.02° different from zero. We therefore conclude that in this respect ve23 - ve25 are very accurate, whereas cases ve21a and ve22a are not so accurate.

- For the very narrow directional distribution used in ve28, the computed wave directions behind the bar are also not as accurate as might be expected, $\theta_c = 0.19°$.

- An explanation for these noted inaccuracies (compared to the other cases) might be the discretization in θ; for the narrow directional distributions a discretization of $5°$ has been chosen, while for the other cases $7.5°$ has been taken, see section 3.3. With the directional spread σ of $12.5°$ and $25.0°$ for the exponents m=20 and m=4 respectively, the rates $\sigma/d\theta$ become 2.50 and 3.33. This means that the wider directional distribution is in fact represented more accurate than the narrower one.

- In ve28 has been used $d\theta = 2.5°$, giving the rate $\sigma/d\theta = 6.83/2.5 = 2.73$; that ve28 gives more accurate results for θ_c than does ve22a is thus consistent with the better discretization for ve28.

- Investigating the computed principal wave directions at line 7), furthest from the wavemaker, we notice the following (small) deviations from the expected values which should be zero. The deviations at site 29, lying midway between the sidewalls, are explained above to be to some extent an effect of too crude discretizing in θ and difference in refraction. On line 7) we notice for cases ve21a, ve22a, ve23-ve25 a decrease of θ for decreasing y (thus, a decrease from site 27 to 39 to 29 to 28). This variation is due to the condition of fully absorption at the sidewards boundaries. This condition acts as an attractor of energy, and the computed results are thus consistent with this cause. We notice that the effect is larger for the wider directional distribution, as is clear from a comparison of the results of ve23-ve25 with those of ve22a. Furthermore, the effect is not visible in the results of ve28, the case with a very narrow directional distribution, which is as expected.

3.4.5 Directional spread.

A comparison of the computed and measured directional wave spreading is a difficult task, foremost because the spreading measures are different in the two cases, see appendix F. In Table E.37 the results of the primary statistical parameters have been given for the seven sites where measurements are available. From the values of the index of agreement and the modified index of agreement it is clear that for these measures of directional spread a rather low correspondence is found. This is especially true

when comparing the values d and d1 found here with those for the wave height at the same seven sites as are given in Table E.15.

A better picture of the situation for the directional spread may be obtained by considering the point by point comparison as given in appendix Q. Focussing attention on the cases ve21a, ve22a, ve23, ve24 and ve25, we notice the following.

- For the low wave height case, ve21a, a slight broadening of the directional distribution behind the bar is observed (from $12.5°$ to $14.1°$). In the corresponding measurement, me21, the directional spread measure, σ_m, increases from $18°$ to $26°$, and thus a much larger broadening of the directional distribution is observed in the measurements.

- For ve22a, no broadening is observed, but even a slight decrease in σ_c is obtained. However, for the corresponding measurement, me32, a larger increase of spread is obtained, from $18°$ to $31°$. Notice that cases me21 and me22 were the measurements for a two-dimensional spectrum which was narrow in both frequency and directional distribution.

- For the cases with a wide directional distribution, me23, me24 and me25, the directional spread obtained in the measurements is increasing from $26°$ in front of the bar to $37°$ behind the bar, irrespective of the width in the frequency distribution close to the wavemaker (peak enhancement factor γ_o = 7, 1 and 3.3 for me23, me24 and me25 respectively). For the computations ve23, ve24 and ve25 the same pattern for the spread σ_c is obtained, as it should be. The directional distribution is the same in the three computations and the computations proceed with effectively one (mean) wave period, there is no frequency distribution as such present in HISWA. However, the directional spread σ_c decreases from $25°$ in front of the bar to $20.5°$ behind the bar.

- A simple geometric interpretation of the behaviour of the directional distribution in the case of refraction of wave on straight parallel iso-baths has been given by Longuet-Higgins (1956), see also Kinsman (1965, p. 352). When considering two waves with the same frequency, but different directions, the angle between the wave number vectors

decreases upon propagation into shallower water. When considering two
wave components with different frequencies, but starting in the same
direction, the wave number vectors do make an angle after propagation
into shallower water. Frequency and directional distributions thus
have opposing effects on the change of the directional spread mea-
sure. Because in HISWA the wave frequencies in the various directions
are almost equal at a certain location in the present situation, the
spreading measure σ_c is expected to decrease from the computational
boundary to a position on the bar. This behaviour is indeed present in
the computational results, see the results in appendix L. So is for
ve21a and ve22a obtained on the crest of the bar (line 4) $\sigma_c = 8°$
while in front of and behind the bar $\sigma_c = 12.5°$.

-   The explanation that in cases ve23 to ve25 the spread behind the bar
    is less than the one in front of the bar is as follows. On the bar the
    wave period decreases due to wave breaking and the refraction effect
    from the crest of the bar to the horizontal region behind the bar is
    therefore less than it was upon climbing the bar. With less refraction
    effect the change in directional spread is therefore also less.

-   Remains to be explained why, in ve21a, the spreading increases from
    12.5° to 14.1°, while the wave period decrease is less than in the
    higher wave height cases. For ve21a the wave period changes from 1.21
    to 0.97 s, while for ve22a the change is from 1.22 to 0.78 s, see ap-
    pendix J. Notice moreover that for ve23 - ve25 the wave period at line
    7) is 0.77 s, while the start wave period ranges between 1.15 and
    1.20 s.

The semi-cylindrical bar geometry.

The measurements with the small directional spread, me31 and me32, show an
increase in the spread σ_m from in front of to behind the bar, see appendix
Q. Because this increase is 7 to 10°, it is assumed to be significant. For
the mesurements with the wide directional distribution, me33-me35, the
directional spread remains nearly constant. Only at site 28 a larger value
is obtained (34.5° versus about 28°); this is most probable due to reflec-
tion effects of the near-lying side-wall.

For the computations ve31-ve34 and ve35b we notice a systematic increase in

σ_c on line 7) from site 39 to 29 to 28; so we have for ve31 respectively 16°, 21° and 25°. In the measurements such a systematic increase in spread does not occur between sites 39 and 29.

For the computations with current, ve35s1 and ve35s2, the calculated directional spreading behaves in a similar manner as in the measurements. In fact, the calculated and measured directional spreading come very close to each other, especially when the difference in intial value is taken into account. So, also for the performance of prediction of the directional spreading, the inclusion of effects of current refraction is important in the present situation.

3.5 Discussion.

The results of the verification of the wave propagation program HISWA with measurements in a wave basin have been reported in this chapter. A principal difference between HISWA and the measurements is that in HISWA the computation proceeds with a single wave period T which is considered to be a characteristic mean wave period for the variance density E(f). This measure for the wave period results from averaging over the frequencies. The propagation velocities as the group velocity are evaluated at this mean frequency, instead of averaging the velocities over the frequencies, which average depends on the spectral shape which is chosen. The difference between averaged velocities, as used in the formulations of the model and the simple evaluation at the mean frequency can amount to 10 % for wider spectra such as the Pierson-Moskovitz spectrum. Some results are given in appendix T.

In verification studies for mathematical models deviations between computed and measured values may be due to several distinct causes. In the first place the description of the physics by the mathematical model has to be looked into; deviation between description and reality generates errors in the socalled "physical accuracy". As it is an impossible task to describe nature in all its details in a mathematical model which can also be solved numerically or otherwise, a choice has to be made concerning the physical causes of primary importance for the applications of interest. The consequence of such a choice is that the mathematical model should only be applied for the physical situations for which it is designed. As HISWA is a

wave propagation program in which the geometric optics approximation is used for the wave propagation part, care should be given to use it only for bottom geometries which do not change too abruptly and are rather smooth. Because HISWA is a refraction program on a grid, concerning the wave propagation part, not too steep slopes should be present in the bottom geometry. Because of the discretizing in the direction, where variations of $60°$ are usually taken with the mean intial wave direction, the problem of trapped waves occurs quite soon for increasing depth situations. Such trapped wave behaviour can be prevented by choosing very small computational steps in the main wave propagation direction; notice that with small steps the difference in water depth is also small and for small differences in depth the occurrence of trapped waves within that step is prevented.

Besides the notion of physical accuracy, we also consider the numerical accuracy. With numerical accuracy we denote the accuracy with which a certain mathematical model is solved numerically. The question of numerical accuracy is best resolved by comparison of computed results with analytical ones; the problem is that in most instances no analytical solutions are available, and if they are, they are usually only available for a subset of the full mathematical model. Therefore it is wise practice to get some idea about the numerical accuracy by variation of computational step sizes, but a real answer is not provided by such a procedure.

A third source of inaccuracy is the incomplete schematization of the input conditions, incomplete in that indeed only a schematization of incoming waves is made. Also when the two-dimensional spectrum of the waves is given as input along the whole of the start line for the computations, the schematization is incomplete in that no distinction is made between linear and non-linearly-coupled waves. Such schematization errors are unavoidable and are related to the mathematical modeling of physical reality. Furthermore, measurement errors are also of importance.

In the present verification study only the combined effect of the various sources of inaccuracies are considered, although the computational parameters have been chosen carefully in most instances. So has the computational step in the main wave propagation direction been chosen rather small to prevent the occurrence of trapped waves and the prediction of negative values of wave action. The choice of the physical parameters such as the wave breaking parameter and the bottom friction factor has been discussed

extensively. It has been argued previously that the bottom friction factor should have been chosen larger so that more dissipation due to bottom friction would result, whereas the wave breaking parameter should also have been chosen somewhat larger, resulting in less dissipation due to wave breaking. A difficulty in the comparison between measurements and computations is due to different boundary conditions. While for the measurements fully reflecting sidewall conditions are appropriate, as can also be seen from an ivestigations of the measurements, in the computations another condition has been taken for the sideward boundaries, as discussed below. The influence of these different boundary conditions plays a role in the verification. Taking all these differences into account, the results of the verification of HISWA are indeed quite good, especially concerning the predicted wave heights.

The principal conclusions of the HISWA verification computations are summarized below. For a more extensive discussion is referred to the foregoing sections.

For the prediction of the wave heights in the present situations HISWA gives quite good results, especially when accounting for current refraction in the computations due to the wave-driven currents as generated in the wave basin. For the fully cylindrical bar geometry the predicted wave heights are more accurate than for the semi-cylindrical bar; in the latter situation errors due to refraction according to the geometric optics method are of more importance. Due to the smearing-out of the results (compared to ordinary refraction calculations) because of the accounting for directional spreading, the computed wave fields are rather smooth. This follows also by a comparison with results of the parabolic model CREDIZ, for which model results have been given in next chapter for a few situations, all for the semi-cylindrical bar. Another reason for the smoothness of the results is the large computational step taken in the lateral direction : dy = 1 m, whereas the step dx in the main wave propagation direction is only 0.10 m.

The computations for the fully cylindrical bar geometry also served the purpose of checking the numerical accuracy of HISWA to some extent; for this reason use was made of the symmetrical situation of normally incident waves. The observed deviations, clearest seen in the wave directions, were indeed very small, but were consistent with what one might expect. It appeared that the discretizing in the direction is also of more importance

than considered at first, at least to obtain (numerically) accurate re-
sults. We suggest for the choice of dθ, in relation to the measure of di-
rectional spread as used in the program, σ, to take the step dθ not larger
than is given by the ratio σ/d$\theta \geq 3$.

As is usual in wave propagation programs, the conditions for the sidewards
boundaries are difficult to devise. In the HISWA version we worked with, in
fact the only possible sidewards boundary condition was the fully absorbing
one, which condition is most accurate when waves are normally incident to
the boundary. As this condition works as an attractor of wave energy, which
is felt over some distance, a condition which allows waves to leave the
computational area unhindered, with low reflection, is often to be prefer-
red; the problem is that such a condition is very hard to implement for
dispersive waves. Another problem is that waves cannot enter the computa-
tional area, as they do in nature. One facility has been built in HISWA to
make this possible to some extent; one can enforce the wave height at the
sidewards boundaries beforehand; the problem, however, is that the choice
of wave height along the sidewards boundaries is in fact not good possible
beforehand in realistic situations. In the present verification study, with
waves generated in a closed wave basin, a reflecting sidewards boundary
condition would be perfect; at the time of performing the computations this
facility was not available, but now it is. Because of the dissipating boun-
dary condition, the lateral extent of the computational domain has to be
chosen quite a bit larger so as to obtain trustworthy results in the region
of interest. As this is also necessary in the parabolic program CREDIZ, the
same socalled perturbed area as in CREDIZ is taken in HISWA to be valid,
i.e., a region with apex of 20° along the sideward boundaries; it has not
been checked whether this is also sufficient for HISWA. We performed a test
for the empty basin and looked for wave directions 1° off from the
theoretical ones; in that situation a perturbed region with apex of 20° was
obtained. The performance of HISWA has been described by means of a set
statistical parameters describing the deviation between measurement and
computation.

Wave height prediction.

The conclusions for the wave heights are primarily based on the results of
17 sites on and behind the semi-cylindrical bar. For the various measuring
conditions the results are discussed in detail in section 3.4.2.

Fully cylindrical bar geometry.

For the normal wave incidence cases ve2x we have as general result that for the fully cylindrical bar geometry the bias is very low (around -1 %) and the deviation measures mae and rmse are 3.5 and 4.4 % respectively. The measures for the overall performance of the predictions, the index of agreement d and the modified index of agreement d1, give values near 1 and around 0.91 respectively. So, for the fully cylindrical bar geometry HISWA performs very good with respect to wave height prediction.

Semi-cylindrical bar geometry.

For the semi-cylindrical bar geometry the performance of HISWA is less; this is partly due to the presence of wave-driven current fields in the wave basin, which are generated by wave breaking. Taking current refraction due to these current fields into account resulted in a great enhancement of the predictive possibilities of HISWA with regard to wave height prediction as is shown in the performance of computations ve35s1 and ve35s2 compared to the case without current refraction, ve35b. The results for the standard normal wave incidence cases are for measuring conditions 1-5 (see Table 3.4) bias = -6.9 %, mae = 9 %, rmse = 10.7 % and the indexes of agreement are d = 0.9 and d1 = 0.7. It is seen that the case without directional spreading, ve38, performs best (bias 0.6 %, mae = 7.5 % and rmse = 9.4 %) while this was not true for the computations ve2x. The computation ve35b has been redone with current refraction (ve35s1 and ve35s2) and also with a higher wave breaking parameter (ve35c). Both effects, taking a higher value for the wave breaking parameter and taking current refraction into account yield better performance of HISWA as is shown for a few parameters for the wave height in the Table below. As comparison, the results for ve25 have been added.

	ve35b	ve35c	ve35s1	ve35s2	ve25
bias (%)	-7.8	-4.4	-3.2	-4.3	-1.3
mae (%)	9.7	7.5	4.0	4.9	3.8
rmse (%)	11.1	8.8	5.2	6.1	4.5
d	0.92	0.94	0.98	0.97	0.99
d1	0.72	0.77	0.86	0.83	0.92

It is conjectured that the combination of a higher wave breaking parameter and accounting for current refraction yields even better performance.

Wave period predictions.

For testing the performance of characteristic wave period prediction in HISWA the fully cylindrical bar geometry is especially suited. For verification of the wave period we have seven sites available, of which three sites are situated close to the wave maker, one is situated on the tip of the semi-cylindrical bar and three are behind the bar. So in fact only four sites can be used for testing the predictive capabilities of HISWA for the wave period. For the computations ve2x the result is that the wave period behind the bar is about 30 % too low, compared with the corresponding wave period measure as obtained from the variance densities. Taking a constant wave period would result in a better performance and it is thus concluded that the algorithm for adapting the wave period due to wave dissipation is unsuitable in its present form. On the one hand a very simplistic spectral form is assumed in HISWA to account for the change in frequency and on the other hand measurements show that considerable secondary peaks develop in the spectrum after wave breaking. This is not only true for the present laboratory experiments, but also occurs in nature, e.g. in the Haringvliet region, for which situation spectra have been shown in Dingemans (1983) and in Dingemans et al. (1984); the same kind of behaviour of the variance densities was seen there as in the present laboratory experiments. Notice moreover, that these secondary peaks generally are not second harmonics peaks, sothat non-linearity is not the only cause of the development of these peaks.

Wave directions.

For the prediction of wave directions it is essentially that current refraction is taken into account in the situations where currents are present as wave-driven currents or as tidal currents. Taking into account that the measured wave directions are at most 4° in error, the performance of the wave direction prediction is less satisfactory than that of the wave heights. Especially for the wave directions the dissipating sidewards boundary conditions have much influence when these are chosen too close to the region of interst.

For a discussion of the performance of the directional spread prediction is referred to chapter 6.

4. Confrontation of CREDIZ computations with measurements.

4.1 Introduction.

In this chapter the results of some computations with the parabolic wave propagation model CREDIZ are reported. These computations serve as a comparison with the HISWA computations. The model CREDIZ has been verified with a number of different measuring conditions, both from the field and from several laboratory conditions, see Dingemans et al. (1984) and Dingemans (1983, 1985). The principal differences between CREDIZ and HISWA are the parabolic wave propagation in CREDIZ versus the geometric optics approach as used in HISWA, and the directional wave distribution as used in HISWA whereas no directional distribution is present in CREDIZ. Furthermore, some effect of non-linearity on the wave propagation characteristics is possible in CREDIZ, with remarkable results as shown in Dingemans and Radder (1986), whereas the wave propagation part in HISWA is purely linear. In CREDIZ the (absolute) wave frequency is constant in the whole of the computational region.

	HISWA	CREDIZ
lateral diffraction	-	+
directional spread	+	-
non-linearity	-	+
variable frequency	+	-

4.2 Overview of the CREDIZ computations.

CREDIZ computations are carried out for the cases of low wave height (me31), narrow frequency and directional distributions (me32) and the "standard" case me35. In the latter case the influence of current refraction is also considered. As in CREDIZ three different boundary conditions for the sidewards boundaries are possible, viz., 1) fully reflecting, 2) nonreflecting for a certain angle, and 3) dissipating, effects of these conditions have also been considered. Notice that in HISWA only the dissipating boundary condition is available.

In CREDIZ sometimes amphidromic points are obtained, whereas in HISWA this is usually not the case due to the smearing out of the wave height field due to the directional spread. A simple trick to reduce the strong wave height variation in the neighbourhood of an amphidromic point is to account for effects of wind; the presence of wind is most felt on the low wave height and much less on the higher wave heights, from which a smearing out of the wave height field results in the neighbourhood of such points. Therefore, a number of computations have been performed with a wind velocity of 0.2 m/s, which value is too low to generate significant wave growth. The computational mesh given by dx' and dy' for CREDIZ should be chosen as dx' $\leq$ L/4 and dy' $\leq$ L/6, where L is a characteristic wave length in the computational area. Initial computations with CREDIZ were performed with wrongly chosen computational mesh, viz., with the mesh as has to be chosen for HISWA. For the depth h = .40 m and T = 1.24 s we obtain L = 2.03 m. The opportunity has been taken to study the sensitivity due to various choices of the mesh size. In all CREDIZ computations the effect of non-linearity on the wave celerity has been included.

The various CREDIZ computations are given in Table 4.1 together with the main computational parameters. It is noted that for the wave period is taken the peak period Tp, not Tm-10 as was used in HISWA.

CREDIZ computations. In the following Table also the computational area has been given by means of the coordinates of its origin A' in terms of bottom coordinates, together with the lengths A'D' in x' and A'B' in y' direction. In the colum marked "bound." the boundary condition along the sidewards boundaries have been denoted by codes as are used in the CREDIZ program; here "2 20" denotes the condition which is usually taken when waves may leave the computational area with direction of 20° with the positive x'-axis; see the end of section 2 in Dingemans et al. (1984) or page 94 in Dingemans (1985). The code "1" denotes fully relfecting boundaries and "3" denotes fully dissipating sidewards boundaries. It is noticed that in HISWA only the fully dissipating boundary has been used as the other two possibilities have not been implemented in HISWA.

case	H	T	gamma	xA'	yA'	A'D'	A'B'	dx'	dy'	bound.	cur.	wind	block
	cm	s		m	m	m	m	cm	cm			m/s	m
ce31	5.08	1.254	.6935	5.0	5.0	31.5	50.0	10	100	2 20	-	-	.5
ce31a	5.08	1.254	.6935	5.0	5.0	31.6	50.0	40	40	2 20	-	-	.5
ce31b	5.08	1.254	.6935	5.0	5.0	31.6	50.0	20	13.2	2 20	-	0.2	.5
ce31c	5.08	1.254	.6935	5.0	16.8	31.6	26.4	20	12.5	1	-	0.2	3.0
ce32	10.06	1.241	.8157	5.0	5.0	31.5	50.0	10	100	2 20	-	-	.5
ce32a	10.06	1.241	.8157	5.0	5.0	31.6	50.0	40	40	2 20	-	-	.5
ce32b	10.06	1.241	.8157	5.0	5.0	31.6	50.0	40	40	2 20	-	-	3.0
ce35	10.42	1.17	.8385	5.0	5.0	31.5	50.0	10	100	3	-	-	.5
ce35a	10.42	1.241	.8213	5.0	5.0	31.5	50.0	10	100	2 20	-	-	.5
ce35b	10.42	1.241	.8213	5.0	16.8	31.6	26.4	40	25	1	-	-	.5
ce35b1	10.42	1.241	.8213	5.0	16.8	31.6	26.4	20	12.5	1	-	0.2	.5
ce35ba	10.42	1.241	.8213	5.0	16.8	31.6	26.4	20	12.5	1	s1	0.2	.5
ce35bb	var	1.241	.8213	5.0	16.8	31.6	26.4	20	12.5	1	s1	0.2	.5
ce35bc	var	1.241	.8213	5.0	16.8	31.6	26.4	20	12.5	1	s1	0.2	3.0
ce35s1	10.42	1.241	.8213	5.0	5.0	31.5	50.0	10	100	2 20	s1	0.2	.5
ce35sa	10.42	1.241	.8213	5.0	5.0	31.6	50.0	40	40	2 20	s1	0.2	.5
ce35sb	10.42	1.241	.8213	5.0	5.0	31.6	50.0	40	40	2 20	s2	0.2	.5
ce35c	10.42	1.241	.8213	5.0	5.0	31.6	50.0	40	40	2 20	-	-	.5

Table 4.1 Overview of CREDIZ computations.

Comments on the various computations.

ce31   wrong computational mesh sizes dx' and dy'.

ce31a   reduced values dx' and dy'.

ce31b   small values dx' and dy'; some wind influence; this is the case primarily to be compared with the measurement me31.

ce31c   fully reflecting sidewards boundaries have been applied; small computational area (the same as the physical basin); larger averaging blocks have been used.

ce32   wrong computational mesh sizes dx' and dy'; reasonable values for dx' and dy' are used in ce32a and ce32b; in ce32b larger averaging blocks have been used.

ce35   wrong computational mesh sizes dx' and dy' have been used; dissipating sidewards boundaries have been used.

ce35a   wrong computational mesh sizes dx' and dy' have been used; nonreflecting sidewards boundaries have been used; results of ce35 and ce35a should be compared to each other.

ce35b   correct values for dx' and dy' have been used; results of ce35b should be compared with the corresponding HISWA computation ve35b.

ce35b1 small values dx' and dy' have been used; also some wind influence has been added in order to reduce the effect of amphidromic points (especially to study the influence oon the wave height at site 29).

ce35ba as computational area the physical basin has been taken and fully reflecting boundaries have been applied; the measured current field (s1) has been taken into account; wind velocity of .2 m/s has been applied; small mesh sizes dx' and dy' have been taken.

ce35bb the setting is as in ce35ba, but now with a variable wave height along the start boundary to comply with the variable wave height distribution as found in the measurements; there have been applied the following wave amplitudes H at positions y along the start line, denoted as the following pairs, with y in m and a=H/2 in cm: (16.8, 5.02), (25.0, 5.02), (30.0, 5.22), (40.0, 5.63), (43.2, 5.63); notice that for intermediate values y the wave amplitude has been interpolated linearly.

ce35bc as ce35bb, but now with larger averaging blocks; the influence of the dimension of the averaging blocks can be ascertained from a comparison of the results of ce35bb and ce35bc; the results of ce35bb and ce35bc are also to be compared with the results of HISWA computations ve35s1.

ce35s1   50 m wide computational region; the mesh sizes dx' and dy' are
         wrong current field s1 has been taken into account.

ce35sa   correctly taken computational mesh sizes dx' and dy'; current
         field s1 has been taken (i.e., the current field is zero outside
         the boundaries of the physical basin).

ce35sb   as ce35sa, but now the current field s2 has been taken into acount
         (i.e., the current field has been extended outside the boundaries
         of the physical basin); results of ce35sa and ce35sb are directly
         comparable to results of the HISWA computations ve35s1 and ve35s2
         respectively.

ce35c   no current; dx' and dy' are .40 m; this computation in fact repla-
         ces ce35a.

4.3 Discussion of results of the computations.

4.3.1 Introduction.

The discussion of the performance of the CREDIZ computations follows the
same lines as in the case of the HISWA computations, see section 3.4.1. As
this report is in first instance a report on the performance of HISWA, the
results of the CREDIZ computations are not discussed so extensively as
might have been done; however, all pertinent data has been given so as to
make it possible for the interested reader to draw his own conclusions.
Here, we are primarily concerned with the differences in performance of the
two wave propagation models HISWA and CREDIZ, while using the same measure-
ments as a yardstick. We first concentrate on the statistical parameters
concerning the wave heights at the measuring sites; results have been given
in appendix E, Tables E.17 to E.32. For the discussion we mostly concentra-
te on the situation where 17 measuring sites on and behind the semi-cylin-
drical bar have been taken into account, see Tables E.23 and E.24. The
relative errors for all sites have been given in appendix M.

As a number of computations have been performed with incorrect values for
the computational mesh size, we do not discuss all computations, but focus
the attention to those computations in which correctly chosen parameters
have been used. As it can be argued that an averaging block with sides of
0.5 m is rather small, especially for use in monochromatic wave propagation
programs without directional spreading as CREDIZ is, also larger averaging
blocks have been chosen for a number of computations; the sides of these
larger blocks have been chosen as 3 m, about 1.5 to 2 times the wave length
as it is reasonable to average results over several wave lengths. Notice in
this connection that for verification purposes in nature as described in
Dingemans (1983) and Dingemans et al. (1984) averaging blocks of 250 m were
taken, while a characteristic wave length was about 60 m. In the following
discussion of the results of the CREDIZ computations attention is focussed
on the three items : 1) the performance of CREDIZ in relation to the mea-
surements, 2) the difference in performance of CREDIZ and the corresponding
HISWA computation and 3) the sensitivity of the results for variation in,
e.g., the sidewards boundary conditions. In the discussion the following
combination of cases are considered.

ce31b and ce31c   to study the influence of reflecting boundaries;
                       results of ce31b are to be compared with case ve31;

ce32a and ce32b   intercomparison yields the influence of the averaging
                       block size;

ce35b and ce35b1   to study the influence of small wind velocity;

ce35ba and ce35b1   influence of current refraction; current distribution
                       s1;

ce35bb and ce35ba   influence of varying wave height on start boundary;

ce35bc and ce35bb   influence of averaging block size;

ce35sa and ce35sb   current fields s1 respectively s2; these cases are
                       directly comparable with HISWA computations ve35s1 and
                       ve35s2; no reflecting boundaries.

4.3.2 Wave height.

General discussion of the wave height results of CREDIZ.

The wave heights at the sites have been compared with the measured ones in scatter plots, one for each computation, in which all 26 values have been given; see Figures 48 to 65.

Considering the values of the index of agreement, d, as are given in Table E.23, it is noticed that the cases of the low wave height (measuring condition me31) perform much less than the other cases for higher waves. The same phenomenon was found for the HISWA computations (see Table E.7). Whereas for ve31 there was obtained d=0.72, here we have for ce31b, d=0.60, and CREDIZ gives thus a much lower performance here. Notice that for fully reflecting boundary conditions, case ce31c gives d=0.73. The relative deviations as given in appendix M show that for ce31b and ce31c one site, site 29, gives very bad results, a deviation of -58 % for ce31b and -39 % for ce31c; for ve31 such outliers are not obtained. It is concluded that near site 29 an amphidromic point in the CREDIZ computations is obtained.

In order to see the influence of one very inaccurate value on the total, the statistical parameters are calculated for the sites on and behind the semi-cylindrical bar with site 29 excluded. For the resulting 16 sites the values of the parameters have been given in Tables E.25 and E.26 for the CREDIZ computations and in Tables E.9 and E.10 for the HISWA computations. From Table E.25 it is seen that d = 0.85 and d1 = 0.64 for ce31b, while, when taking site 29 into account, one obtains d = 0.60 and d1 = 0.54 as given in Table E.23. A considerable improvement is also obtained for the regression line when site 29 is not accounted for; this is also clear by considering the scatter plot, Fig. 50.

The intercomparison of cases ce31b and ve31 for 16 sites gives slightly better performance for ce31b when considering the parameters bias, mae, rmse, a, b, sd and the indexes of agreement d and d1. However, this is the case when neglecting the site close to an amphidromic point; for 17 sites, ce31 achieves better. The problem of ocurrence of amphidromic points in the CREDIZ computations remains.

It follows from Table E.25 that the computations for low wave height perform least well of all computations. Furthermore, the case ce31c, for fully reflecting sidewards boundaries, performs -for all combinations of sites considered- better than case ce31b. This is an indication for the importance of reflections in the physical model; notice that the sidewards boundaries consisted of vertical concrete walls.

In the subsequent discussion we will exclude the results of site 29 in first instance and consider therefore the statistical parameters as based on the 16 sites. The results for 17 sites are also given and the CREDIZ computations are compared to the corresponding ones of HISWA.

Specific discussion of the wave height results of CREDIZ.

Cases ce31b and ce31c.

A few of the statistical parameters for ce31b and ce31c taken from Tables E.25 and E.26 and the ones for ve31 from Table E.9 and E.10 yield :

case	n	bias %	mae %	rmse %	pes %	a cm	b	d	d1	r2
ce31b	16	-4.31	7.52	9.58	20.38	-0.38	1.03	0.85	0.64	0.64
ce31c	16	-5.31	6.97	8.32	40.72	-0.15	0.98	0.87	0.66	0.73
ve31	16	-4.51	7.64	9.96	43.50	1.94	0.56	0.74	0.57	0.40
ce31b	17	-7.77	10.77	17.96	20.99	0.87	0.75	0.60	0.54	0.20
ce31c	17	-7.48	9.04	13.12	35.28	0.64	0.80	0.73	0.59	0.40
ve31	17	-5.21	8.14	10.44	49.12	2.11	0.52	0.72	0.54	0.36

Table 4.2 Statistical parameters for wave height.

Based on 16 sites, both CREDIZ computations perform better than the HISWA computation. It is seen that especially the regression is much better for CREDIZ compared to the one for HISWA. Based on 17 sites (with site 29 included) ve31 performs better than ce31b, but also for this case the regression for the CREDIZ computation is markedly better than for the HISWA case. Notice that the modified index of agreement does not show any difference

for 17 sites, but the importance difference lies in the values for the
bias, and the deviation measures mae and rmse and also sd. For sd we have

case	17 sites	16 sites
ce31b	16.69	8.84
ce31c	11.11	6.62
ve31	9.32	9.17

Table 4.3 Values sd for wave height, in %.

The influence of the reflecting boundary conditions, taken in ce31c, is
clearly seen from these results.

Cases ce32a and ce32b.

Basing the conclusion on 16 sites, it is seen from the statistical para-
meters, of which some have been collected in Table 4.4 below, that CREDIZ
performs slightly better than the corresponding HISWA computation. It is
remarked that the measuring condition me32 is the one for narrow frequency
and directional distribution. An increase of the averaging block size, as
is used in ce32b, is seen to yield smaller deviations and a somewhat higher
value of the index of agreement, but a less good regression and a higher
(negative) bias. The higher value for the proportion due to systematic
deviations to the mean square error, pes, indicates that for ce32b a more
optimal parameter setting is possible, whereas, for ce32a a near optimal
setting has been used. It is seen that even for the 17 sites CREDIZ com-
putation ce32b performs somewhat better than HISWA computation ve32.

It is noticed that also for CREDIZ a negative bias is obtained for the
semi-cylindrical bar geometry. For HISWA it has been argued, based on the
fully cylindrical bar results, that the wave breaking parameter has been
chosen too low, also because the bottom friction parameter fw was chosen
too low. The bias was especially negative in the case of the semi-cylin-
drical bar geometry. Considering the sites on the downward slope and behind
the bar, except site 29 (thus the 9 sites), it is seen that the bias for
CREDIZ is less negative than is the case for HISWA (Table 4.5).

case	n	bias %	mae %	rmse %	pes %	a cm	b	d	d1	r2
ce32a	16	-2.55	7.22	9.99	6.54	-0.16	1.00	0.94	0.80	0.80
ce32b	16	-4.01	6.53	8.47	23.40	-0.64	1.04	0.96	0.82	0.88
ve32	16	-5.53	8.34	10.02	30.71	-0.63	1.03	0.94	0.78	0.85
ce32a	17	-4.17	8.60	12.14	12.29	-0.66	1.04	0.92	0.77	0.76
ce32b	17	-4.66	7.04	8.99	28.48	-0.82	1.06	0.95	0.80	0.88
ve32	17	-5.24	7.90	9.79	28.76	-0.52	1.02	0.94	0.78	0.85

Table 4.4 Statistical parameters for the wave height.

case	n	bias %	mae %	rmse %	pes %	a cm	b	d	d1	r2
ce32a	9	-4.93	10.98	13.57	14.97	0.44	0.89	0.85	0.64	0.57
ce32b	9	-7.77	9.64	11.25	48.06	-0.85	1.04	0.90	0.68	0.81
ve32	9	-9.50	11.41	13.15	69.80	1.75	0.66	0.82	0.59	0.69

Table 4.5 Statistical parameters for the wave height.

Cases ce35b and ce35b1.

Computations ce35b and ce35b1 are carried out with fully reflecting side-
wards boundaries. In ce35b1 a small wind velocity (0.2 m/s) has been ap-
plied in order to try to prevent the formation of amphidromic points and to
obtain an otherwise also smoother wave height distribution. From the rela-
tive deviations given in appendix M it is seen that the effect of the wind
is only very slight, also at site 29; at site 29 the error decreases from
-33.2 % to -31.8 %. The statistical parameters show for both 16 and 17
sites a slight increase in performance when some wind is taken into
account, see also Table 4.6 below.

A comparison of CREDIZ computations ce35b and ce35b1 with the corresponding
HISWA computation ve35b shows that CREDIZ performs somewhat better, especi-

ally the bias is much less, but also the deviations mae and remse are smaller for CREDIZ; for the bias and mae this is the case for both the 16 and 17 sites.

case	n	bias %	mae %	rmse %	pes %	a cm	b	d	d1	r2
ce35b	16	-1.75	7.39	9.72	20.59	-2.04	1.24	0.94	0.78	0.85
ce35b1	16	-1.15	7.26	9.71	15.64	-1.81	1.22	0.94	0.78	0.84
ve35b	16	-7.93	9.87	11.28	62.59	-2.54	1.24	0.92	0.72	0.90
ce35b	17	-3.40	8.75	11.92	25.47	-2.60	1.30	0.91	0.75	0.81
ce35b1	17	-2.76	8.55	11.72	20.69	-2.37	1.28	0.91	0.75	0.80
ve35b	17	-7.83	9.67	11.09	61.84	-2.42	1.23	0.92	0.72	0.90

Table 4.6 Statistical parameters for the wave height.

Cases ce35ba and ce35b1.

In case ce35ba current refraction is included in CREDIZ; the current field s1 has been used and fully reflecting boundary conditions have been applied. Also wind of 0.2 m/s has been applied. In order to see the effect of current refraction, this case is compared to ce35b1, which is otherwise the same. The corresponding HISWA computation is ve35s1; here no reflecting boundary conditions and no wind influence have been applied. Some statistical parameters have been collected in Table 4.7 below.

It is clear from Table 4.7 that the CREDIZ computation including current refraction performs less than the one without. From appendix M it is seen that at site 29 the two computations differ significantly : the relative deviation is -31.8 % for ce35b1 versus +25.1 % for ve35ba. In general, it follows from Table 4.7 that the bias for ce35ba is larger (negative) than for case ce35b1; a reason for this could be that the current field used has not checked on its divergence property and the divergence of the current field acts as a further dissipation or generation term in the parabolic model, according to the sign of divU (> 0 or < 0 respectively) see, e.g. Dingemans (1985).

case	n	bias %	mae %	rmse %	pes %	a cm	b	d	d1	r2
ce35b1	16	-1.15	7.26	9.71	15.64	-1.81	1.22	0.94	0.78	0.84
ce35ba	16	-5.16	9.77	11.57	22.97	-1.36	1.12	0.91	0.70	0.77
ve35s1	16	-3.04	3.98	5.18	34.58	-0.22	1.00	0.98	0.86	0.94
ce35b1	17	-2.76	8.55	11.72	20.69	-2.37	1.28	0.91	0.75	0.80
ce35ba	17	-3.57	10.57	12.54	8.64	-0.71	1.06	0.89	0.75	0.80
ve35s1	17	-3.16	4.04	5.18	37.13	-0.25	1.00	0.98	0.86	0.94

Table 4.7 Statistical parameters for the wave height.

The HISWA computation with current refraction performs much better than CREDIZ computation ce35ba. The principal reason for this behaviour is in our opinion the fact that in HISWA the wave period decreases and that in the region on an behind the bar, where the current is the most significant, the effect of current refraction is larger than it can be in CREDIZ where the wave period is fixed on its initial value. Moreover, in HISWA the computation proceeds with a smaller wave period close to the wave maker because Tm-10 < Tp everywhere. So in the HISWA computations inclusion of a current field has always a larger influence on the resulting wave height field than it has in CREDIZ.

Cases ce35bb and ce35ba.

Since the performance of ce35ba was so disappointing, the influence of a variable wave height distribution along the start boundary has been investigated, resulting in case ce35bb; this case is to be compared with ce35ba. As can be seen from Table 4.8 a variable wave height along the start boundary gives no improvement of the performance; in fact a slight decrease in performance is obtained.

case	n	bias %	mae %	rmse %	pes %	a cm	b	d	d1	r2
ce35bb	16	-6.56	10.66	12.13	29.91	-0.98	1.06	0.89	0.67	0.75
ce35ba	16	-5.16	9.77	11.57	22.97	-1.36	1.12	0.91	0.70	0.77
ve35s1	16	-3.04	3.98	5.18	34.58	-0.22	1.00	0.98	0.86	0.94
ce35bb	17	-4.95	11.36	12.94	14.63	-0.33	0.99	0.87	0.64	0.65
ce35ba	17	-3.57	10.57	12.54	8.64	-0.71	1.06	0.89	0.66	0.80
ve35s1	17	-3.16	4.04	5.18	37.13	-0.25	1.00	0.98	0.86	0.94

Table 4.8 Statistical parameters for the wave height.

Cases ce35bc and ce35bb.

The effect of larger averaging blocks is investigated for case ce35bb; in ce35bc larger averaging blocks have been taken and ce35bc is otherwise the same as ce35bb, thus in both cases a variable wave height distribution is taken along the start boundary and current refraction and fully reflecting sidewards boundaries have been applied. The parameters given in Table 4.9 give some improvement for ce35bc compared to ce35bb and ce35bc is also seen to be slightly better performing than the case with constant initial wave height, case ce35ba. HISWA computation ve35s1 performs still far better.

case	n	bias %	mae %	rmse %	pes %	a cm	b	d	d1	r2
ce35bb	16	-6.56	10.66	12.13	29.91	-0.98	1.06	0.89	0.67	0.75
ce35bc	16	-5.83	8.84	9.78	36.74	-0.95	1.06	0.93	0.71	0.84
ce35ba	16	-5.16	9.77	11.57	22.97	-1.36	1.12	0.91	0.70	0.77
ve35s1	16	-3.04	3.98	5.18	34.58	-0.22	1.00	0.98	0.86	0.94
ce35bb	17	-4.95	11.36	12.94	14.63	-0.33	0.99	0.87	0.64	0.65
ce35bc	17	-4.66	9.24	10.19	20.96	-0.47	1.01	0.92	0.69	0.77
ce35ba	17	-3.57	10.57	12.54	8.64	-0.71	1.06	0.89	0.66	0.80
ve35s1	17	-3.16	4.04	5.18	37.13	-0.25	1.00	0.98	0.86	0.94

Table 4.9 Statistical parameters for the wave height.

-80-

Cases ce35sa and ce35sb.

In computations ce35sa and ce35sb the current fields s1 and s2 have been
applied respectively. The computational area is here 50 m wide and the
usual sideward boundary condition has been applied. The wave height is
constant along the start boundary. The results show that cases ce35sa and
ce35sb perform about equally well, see Table 4.10; the case with the cur-
rent field s2, ce35sb, performs slightly better. Comparison with the cor-
responding HISWA computations ve35s1 and ve35s2 shows again a much better
performance for HISWA in this case.

case	n	bias %	mae %	rmse %	pes %	a cm	b	d	d1	r2
ce35sa	16	-5.58	10.08	11.95	25.15	-1.46	1.13	0.90	0.69	0.77
ve35s1	16	-3.04	3.98	5.18	34.58	-0.22	1.00	0.98	0.86	0.94
ce35sb	16	-5.46	9.86	11.63	25.07	-1.38	1.12	0.91	0.69	0.78
ve35s2	16	-4.05	4.69	5.96	46.84	-0.12	0.97	0.97	0.84	0.93
ce35sa	17	-3.99	10.84	12.83	10.36	-0.81	1.06	0.88	0.66	0.68
ve35s1	17	-3.16	4.04	5.18	37.13	-0.25	1.00	0.98	0.86	0.94
ce35sb	17	-3.89	10.63	12.52	10.20	-0.73	1.06	0.89	0.66	0.68
ve35s2	17	-4.25	4.85	6.05	49.48	-0.19	0.98	0.97	0.83	0.93

Table 4.10 Statistical parameters for the wave height.

4.3.3 The wave direction.

The measured and computed wave directions have been given in appendix P for
the seven sites where measurements for the wave direction are available.
Here we consider again the results of the computations as given at the end
of section 4.3.1 in order to study the sensitivity for the parameters; we
also compare the results with the principal wave direction as resulting
from the corresponding HISWA computations. We concentrate the discussion on
the sites on and behind the bar, sites 38, 39, 29 and 28, of which site 38
is considered to be the most important one.

Cases ce31b and ce31c.

Here we consider cases ce31b and ce31c which differ with respect to the sidewards boundary conditions; in ce31c fully reflecting boundary conditions are used whereas in ce31b a wide computational region with the usual outgoing wave boundary condition has been used. Furthermore, different sizes of the averaging blocks are taken, the larger averaging block is used in ce31c. From appendix P we have the following results for the measured principal wave direction, θ_m, and the computed direction, θ_c. The CREDIZ computation ce31b is directly comparable with the HISWA computation ve31.

site	me31	ce31b	ce31c	ve31
38	-28.63	-35.91	-32.06	-32.16
39	-8.70	-18.15	-18.11	-16.31
29	-6.02	-45.87	-33.04	-14.85
28	-8.54	-11.50	-0.57	-13.22

Table 4.11 Wave directions θ.

For site 38, situated on the tip of the bar, the wave directions for ce31b and ve31 are rather close, they differ only 4°. As the wave periods at site 38 are 1.254 s for the CREDIZ computation and 1.155 s for ve31, this difference is not much; this is due to the diffraction effect included in CREDIZ. Notice that we consider here the case of small wave heights, for which the wave propagation should be with a good approximation be linear, and no currents of any importance are generated for this non-breaking wave field. This is the reason that the computed wave directions are close to the measured ones. The influence of the reflective boundary condition in ce31c is clearly seen from the results.

For site 39, lying behind the tip of the bar, the computed wave directions are nearly the same for all three cases, but differ significantly from the measured one. Notice that we consider a deviation for the wave direction from the measured one significant when it is larger than 4°, because 4° is estimated to be the largest error in the measured wave direction, as is discussed before.

For site 29 the CREDIZ wave directions are far off from the measured ones. Notice that this site was identified in last section as lying close to an amphidromic point. For ve31 a deviation of nearly 9° is found. Site 28 lies behind the cylindrical part of the bar, 7.2 m from the sideward boundary. Here the wave directions of the comparable computations ce31b and ve31 are reasonable close to the measured one, with the CREDIZ wave direction somewhat better. For the case with the fully reflecting boundary condition, ce31c, a direction of about 0° is found; it is seen that such a direction is also measured in the situations with higher, breaking, waves, see, e.g., Table 4.12 and appendix P. In the measurement me31, the direction is -8.5° and this is due to diffraction around the tip of the bar, which is larger than for unidirectional waves because of the directional spreading. In the higher wave height cases dissipation due to wave breaking and the thus induced currents is dominant over diffraction effects.

Cases ce32a and ce32b.

Here the influence of the averaging block size on the resulting wave directions can be studied (in ce32b the larger block size has been used). In both computations a wide computational domain has been used with the usual sidewards boundary conditions.

site	me32	ce32a	ce32b	ve32
38	-14.11	-35.38	-31.01	-34.22
39	1.71	-16.42	-16.44	-19.48
29	-4.04	-40.86	-31.46	-23.43
28	-1.45	-13.21	-1.27	-21.21

Table 4.12 Wave directions.

The computed results are, for site 38, not significantly different from the small amplitude case, whereas the measured wave directions are significantly different because of wave induced current generation. The averaging block size has especially large influence at site 28 (apart from site 29 with its own pecularities). From appendix K it is seen that at site 28 the standard deviation due to the averaging is 0.61° for ce32a, while it has the unduly large value of 15.88° for ce32b; this means that the value

-1.27° at site 28 for ce32b has low accuracy and the fact that it is close
to the measured value has not much significance. Again it is seen that at
site 38 the differences between CREDIZ and HISWA are minor, whereas the
difference in wave period at that site are large (T = 1.241 s for CREDIZ
and T = 1.064 s for ve32).

Cases ce35b1 and ce35ba.

Here the difference between computations without (ce35b1) and with current
refraction (ce35ba) are considered. In both computations reflecting bounda-
ry conditions have been applied. These CREDIZ computations are to be compa-
red with HISWA computations ve35b and ve35s1 respectively. The resulting
wave directions have been given in Table 4.13 below.

site	me35	ce35b1	ce35ba	ve35b	ve35s1
38	-13.88	-34.96	-13.43	-33.10	-13.18
39	-3.37	-16.41	-0.77	-19.16	-1.50
29	-9.64	-40.05	9.26	-22.74	-2.86
28	2.32	-13.41	2.03	-21.00	-7.54

Table 4.13 Wave directions.

The improvement due to accounting for current refraction is clearly seen at
site 38. That CREDIZ computation ce35ba performs better at site 28 than
HISWA computation ve35s1 is not only due to the reflecting boundary condi-
tion used in ce35ba, whereas this was not possible in HISWA, where a wide
computational domain had to be used. That the reflecting boundary condi-
tion is not the reason for better performance of CREDIZ becomes clear by
considering cases ce35sa and ce35sb as given in Table 4.15 below.

Cases ce35ba, ce35bb and ce35bc.

Here the influence of a variable wave height on the start boundary (ce35bb)
and the influence of larger averaging blocks (ce35bc versus ce35bb) on the
resulting wave directions are made explicit. The resulting wave directions
have been given in Table 4.14.

site	me35	ce35ba	ce35bb	ce35bc	ve35s1
38	-13.88	-13.43	-13.27	-11.47	-13.18
39	-3.37	-0.77	-0.69	1.98	-1.50
29	-9.64	9.26	9.41	10.12	-2.86
28	2.32	2.03	1.95	0.63	-7.54

Table 4.14   Wave directions.

As the differences between the wave directions resulting from ce35ba and ce35bb are very slight, the variable wave height distribution as chosen here along the start line of the computational boundary has no effect. The averaging block size also has no significant effect on the resulting wave directions.

Cases ce35sa and ce35sb.

In computations ce35sa and ce35sb a wide computational domain has been used and the usual sidewards boundary conditions have been applied. The current fields s1 and s2 have been used in ce35sa and ce35sb respectively. These computations are directly comparable to the corresponding HISWA computations ve35s1 and ve35s2.

site	me35	ce35sa	ve35s1	ce35sb	ve35s2
38	-13.88	-13.38	-13.18	-13.32	-11.62
39	-3.37	-0.20	-1.50	-0.46	2.88
29	-9.64	9.24	-2.86	9.26	-0.23
28	2.32	1.44	-7.54	1.90	-6.07

Table 4.15   Wave directions.

The noticeable feature of these results is that the performance of CREDIZ is so much better at site 28 than that of HISWA. It is believed that this is due to differences in current refraction in CREDIZ compared to HISWA : in HISWA the wave period is much smaller so that the Doppler shift in wave frequency has larger influence in HISWA. Notice that at site 28 the abso-

lute wave period in HISWA is 0.856 s in ve35s1, whereas it is 1.241 s in ce35sa.

4.4 Discussion.

Some CREDIZ computations have been performed for the semi-cylindrical bar geometry. These computations have been performed not so much to determine the performance of CREDIZ itself because enough verification studies already have been performed for CREDIZ, but in order to study the performance of HISWA in relation to another much used wave propagation model. Because in CREDIZ the possibility of applying reflecting sidewards boundary conditions is present, also the possible effect of reflecting conditions in HISWA may be estimated for the present situation. In CREDIZ there is seen an increase in performance when reflecting boundary conditions are applied. For the cases of no current refraction the performance of CREDIZ is about the same as that of HISWA, slightly better if one amphidromic point in the CREDIZ computations is excluded from the considerations. When current refraction is accounted for, the perfromance of CREDIZ is considerable less than that of HISWA; the reason herefore is probably due to the differences in wave periods because of which the currents have larger effect in HISWA than they have in CREDIZ. Another source of difference is the fact that the divergence of the current field has as effect some (positive or negative) dissipation in CREDIZ, whereas this is not the case in HISWA; notice that we did not check the introduced current field on the divergence properties.

5. Details of the wave-induced current computations.

Because the wave-induced current fields have been shown to have a profound influence on the predictive capabilities of HISWA, at least with respect to the predicted wave heights, some information on the current computations is given in this chapter. Here we focus on the program system ODYSSEE, see Officier et al.(1986). The program ODYSSEE can be used for a large number of types of flow computations; the user in fact choses its own set of equations to be solved withon the ODYSSEE framework. For the present, the following equations were used (with $x_1 = x$, $x_2 = y$) :

the momentum equations

$$(5.1) \qquad \frac{\partial u_i}{\partial t} + u_j \frac{\partial u_j}{\partial x_j} = -\frac{1}{\rho} \frac{\partial p}{\partial x_i} + \frac{1}{\rho h}(F_i - \tau_{bi}) + \nu_t \frac{\partial^2 u_i}{\partial x_j \partial x_j} \ , \ i = 1,2$$

and the continuity equation

$$(5.2) \qquad \frac{\partial}{\partial x_j}(hu_j) = 0,$$

where : u_i is the horizontal velocity component in direction x_i, averaged over the depth

h $= z_s - z_b$

z_s : the level of the rigid lid (constant in t and $\vec{x}$)

z_b : the bottom level (constant in t, a function of $\vec{x}$)

F_i : the driving force per unit area [$F_i/(\rho h)$ is the driving force per unit mass]

τ_{bi} : the bottom shear stress component in direction x_i

ν_t : the turbulent viscosity coefficient (constant in t and $\vec{x}$).

The formulation of the bottom shear stress is as follows :

$$(5.3) \qquad \tau_{bi} = C_f \cdot \frac{u_i |\vec{u}|}{h} \left\{ 0.75 + 0.45 \left(\bar{\xi} \frac{\hat{u}_{orb}}{|\vec{u}|} \right)^{1.13} \right\},$$

where $C_f = g/C^2$

$C = 18\ ^{10}\log(12h/k_N)$, k_N the Nikuradse roughness, constant in t and $\vec{x}$

$\bar{\xi} = (\frac{1}{2}f_v/C_f)^{1/2}$

$f_v = \exp(-6.0 + 5.2(a/k_N)^{-0.2})$

$\hat{u}_{orb}$: the amplitude of the orbital velocity at the bottom

$a = (T/(2\pi))\hat{u}_{orb}$: amplitude of orbital excursion at the bottom

T : the wave period.

The parameters used are

$\rho = 1000$ kg/m^3

$\nu_t = 10^{-3}$ m^2/s

$z_s = 0$ m (the reference level)

$k_N = 10^{-3}$ m

$T = 1.25$ s

$g = 9.81$ m/s^2.

The computation has been performed with 30 timesteps of 10 s, starting with $\vec{u} = 0$ in the whole field (a socalled "cold start"). This first current computation is denoted by ve35a because driving forces from HISWA computation ve35a have been used; for further notations see appendix R. A second computation, ve35az, has been carried out for 30 more time steps of 10 s each. Also an ODYSSEE computation in which the mass flux has been corrected for the mass flux generated due to breaking waves has been carried out, ve35am; here is started with the velocity field resulting from ve35a and the computation proceeds for 30 time steps of 10 s each. This mass flux correction has been modelled in the following way.

Supposing that in breaking waves the mass flux above the trough-level to consist of two parts, one due to the progressive character of the breaking waves and one due to the surface roller, the mass flux M can be written as

$$M = \left(1 + 7\ \tilde{Q}_b\ \frac{h}{\lambda}\right)\frac{E_{br}}{c} ,$$

where c is the phase velocity of the waves and $\tilde{Q}_b$ is the fraction of time that the waves are breaking. Notice that $\tilde{Q}_b$ is related to the Q_b as used

in the model for wave energy dissipation due to wave breaking in the fol-
lowing way:

$$\tilde{Q}_b = 7.0 \; Q_b \qquad\qquad ; \quad 0 \; \leq Q_b < 0.1$$

$$\tilde{Q}_b = 1.0 - 548.0(0.3 - Q_b)^{4.67} \; ; \quad 0.1 \; \leq Q_b < 0.3$$

$$\tilde{Q}_b = 1 \qquad\qquad\qquad ; \quad Q_b \; \geq 0.3$$

The continuity equation (5.2) then becomes

$$(5.3) \quad \frac{\partial \zeta}{\partial t} + \frac{\partial}{\partial x_j}\left[hu_j + \rho^{-1}M_j\right] = 0 ,$$

where M_j is the induced mass flux in the x_j direction and $M_1 = M\cos\theta$, $M_2 = M\sin\theta$, with θ the wave direction.

The results of the computation with mass flux correction have been given
in appendix R and it is concluded there that inclusion of this correction
term does not give improvement of the current prediction in the present
situation. For a discussion of the performance of the current computations
is referred to the discussions in appendix R.

To be able to compare the computed current fields with the measured one an
interpolation procedure has to be used sothat the two current components
u_1 and u_2 (denoted also as ux and uy) are obtained at the same locations
as the measured currents. Use is made of a procedure that interpolates
from a random grid to a regular grid and needs a search radius r. The user
has to specify the value of r; some sensitivity of the choice has been
reported in appendix R.

The procedure is as follows.

Within the radius r around the desired location the three nearest point
are taken into account. When these point are within a triangle, then the
interpolation is carried out.
Whenever the desired point lies outside the triangle formed by the three
nearest points, an extrapolation is carried out according to Shephards
method of distance weighted average. When the value at the location lies
outside the range formed by the values at the three points, a fourth point

is searched for and four values are taken into consideration. In the situation that one of the angles of the triangle is too acute (which is specified by the smallest perpendicular smaller than some specified value, here taken as 10 cm) then two more points are searched for and a new triangle is formed from which the required value is interpolated.

6. Summary, conclusions and recommendations.

Summary.

For the verification of the wave propagation model HISWA, measurements have
been performed in a wave basin. As HISWA is a refraction program on a grid
in which also discretization in the directions has been applied, it was
essential that the laboratory experiments were conducted with directional
spreading. For this reason the new facility of Delft Hydraulics has been
used in which it is possible to generate two-dimensional spectra. A bottom
geometry has been chosen such that various aspects of HISWA could be tested
on its performance for wave behaviour prediction. The chosen bottom confi-
guration consists of a semi-cylindrical bar with a rounded tip on which
considerable wave breaking is expected, while the tip makes it possible to
test the refraction properties of the program. Newly developed instruments
for measuring two-dimensional spectra (socalled GRSM's) have been used in
the experiments; only three of these instruments were available. As the
data collection was only possible for 16 channels simultaneously, the need
for repeating of experiments for the same input conditions existed. Using
the three GRSM's and seven wave gauges the wave elevations have been measu-
red at 26 sites and the wave directional properties have been measured at
seven sites; one GRSM was taken at a fixed location, close to the wavemaker
and one wave gauge was also taken at a fixed position. To test the perfor-
mance of the wave generation in the wave basin also a simpler geometry,
consisting of a fully cylindrical bar, has been applied for the same measu-
ring conditions. Also a bottom with fixed depth of 0.40 m (the socalled
empty basin) has been applied to test the wave behaviour in the basin in
order to obtain information about the variability of the waves.

Measuring conditions have been varied around two cases : the case of a two-
dimensional spectrum narrow in both frequency and direction and one with a
mean JONSWAP-type of variance density and a reasonable wide directional
distribution (respectively cases 2 and 5, see Table 2.3). In one case (con-
dition 1) small wave heights have been applied and in one case (condition
8) no directional distribution was applied, but long-crested waves have
been generated. The eight measuring conditions chosen give a fair range of
wave conditions for which the wave propagation program HISWA can be tested
on its performance on wave behaviour prediction possibilities.

The HISWA computations performed for the semi-cylindrical bar geometry (computations ve3x) and the ones for the fully cylindrical bar geometry (computations ve2x) have been reported in chapter 3. The results of the computations have been given in terms of the wave heights at the 26 sites and in terms of the wave period, the principal wave direction and the directional spreading at the seven sites on which the directional meters have been applied in the wave basin. The comparison with the measured values has been discussed in chapter 3. For evaluating the performance of HISWA a series of statistical parameters have been calculated, one of which is the index of agreement as introduced by Willmott (1981, 1984). These parameters give results for the performance in a region of space. Apart from such spatial measures also point by point comparisons have been given, especially for the wave parameters for which not much measurements are available. The wave heights as resulting from HISWA have been compared with the wave height HmO as obtained from the variance of the surface elevation. As in HISWA the wave frequency is parameterized as the mean frequency as obtained from the spectral moments m-1 amd mO, the wave periods have been compared with the corresponding wave periods as obtained by calculating these moments from the variance densities of the surface elevation. For the comparison of the principal wave direction and the directional spreading the situation is more difficult; here we are obliged to use different measures in the numerical computations and in the measurements. This is due to the chosen definitions in the program and in the data processing techniques. In the data processing the wave directions are obtained from a Fourier expansion of the directional function and the first few Fourier component amplitudes can be obtained from the one surface elevation signal and the two orthogonal horizontal velocity signals at a given depth. The various definitions have been discussed in appendix F.

In first instance, as part of the Applied Research Programme of Rijkswaterstaat (TOW), current measurements have been performed for two measuring conditions for the semi-cylindrical bar geometry. The distribution of the wave-driven current field has been measured in the whole wave basin at 81 locations in a 3 by 3 m grid. This current field has been used to study the influence of current refraction in HISWA on its performance and it has been shown that inclusion of current refraction in the present situation greatly enhances the performance of the predictive qualities of HISWA. The measured current fields have been given in appendix D. As part of another project, an initial current computation has been performed using the driving forces

obtained from HISWA. As is the case with such initial computations, other cases have been investigated later and care has to be exercised that such initially set up computations do not lead to a project in itself, without changing the computational grid for example. The parameter setting for these current computations (performed with the programming system ODYSSEE) has been given in chapter 5, where also a discussion on the performance of these current computations has been given (see also appendix R).

In order to get a feeling for the performance of HISWA in the present situation in relation to other available wave propagation programs, also computations with the parabolic model CREDIZ have been carried out for a few measuring conditions and the results of both CREDIZ and HISWA have been compared, also in relation to the measurements, in chapter 4. The use of CREDIZ gave also the opportunity to test the sensitivity of different boundary conditions, especially the reflecting boundary condition for the sidewards boundaries.

Detailed results of the measurements have been given in a number of appendices, C, D and S. The values as resulting from the computations have been collected in appendices H to L and comparison of measured and computed wave parameters have been given in appendices M to R.

It has to be stressed that the present verification study is especially valid for bar-typed bottom geometries; the validity of HISWA for coastal regions with a more or less uniformly decreasing water depth in the direction of the coastline has not been investigated. One of the important differences in the two situations is that in the latter case no local wave breaking zone can be defined because once wave breaking starts, it only stops at the coastline. In the bar-typed bottom geometry the dissipation due to wave breaking is a much more localized phenomenon and is therefore easier to model. One has to be aware of the fact that the method of accounting for dissipation due to wave breaking is based on energy balance considerations and it is good possible to get a very good wave height prediction behind a wave breaking zone, but within the wave breaking zone the local wave height prediction may deviate considerably from the local wave height measurement. This is because the performance of the wave breaking model depends critically on the correct setting of a few parameters (in fact only a single one is used in normal circumstances); small changes in that parameter may shift the zone of principal wave breaking a few hunderd meters, but the resulting

wave height behind that zone is not so sentitive to small changes in the value of the wave breaking parameter.

Conclusions.

The performance of the predictive quality of the wave propagation program HISWA is considered in terms of the quality of the prediction of the values of the wave parameters. In this study we consider as wave parameters the wave height, the wave period, the principal wave direction and the directional spreading of the waves. An extensive discussion has been given in section 3.5 and therefore only a few remarks are made here.

The wave height.

For the simple situation of the fully cylindrical bar geometry the wave heights on and behind the bar are predicted with small characteristic deviations in terms of relative measures of bias and root mean square error; a bias of about -0.5 % and rmse about 4.4 % are obtained.

These values are those for the normal wave incidence cases. This correspondence has been achieved with a somewhat too low bottom friction factor f_w, which was taken as 0.01 for all computations, while later analysis showed that it should be taken as about 0.05 for this laboratory case, especially behind the bar, see section 3.2. The wave breaking parameter γ had been set to its socalled optimal setting, which setting has been determined from a collection of different data sets in prototype and laboratory; the optimal value has been found by applying a model with fixed frequency. As an optimal setting for HISWA, where in fact the same wave breaking model is applied as in other programs with fixed frequency, has not been determined, the available optimal setting has been applied.

We have the impression that both opposing effects (too low dissipation due to bottom friction and too high dissipation due to wave breaking) do balance to some extent, especially on these small propagation distances.

Due to the decreasing wave period T in dissipation zones (either due to bottom friction or due to wave breaking), the dissipation due to wave breaking is higher in HISWA than in fixed wave period programs. This indicates that in HISWA at least a somewhat higher wave breaking parameter γ has to

-94-

be applied than in the other programs. The argument that the same wave breaking dissipation formulation as in fixed frequency programs may be applied in the changing frequency program HISWA because in nature the wave period decreases after the surf zone, is not a valid one in all circumstances. As is well known, the peak frequency of spectra remains rather constant in near-shore regions up to the surf zone where considerably wave breaking takes place (the region where wave-driven currents are of importance). In our opinion this is due to the counter effect of non-linear interactions in the spectrum which result in a downward frequency shift; together with the upward shift due to dissipation (primarily due to bottom friction) these effects may balance each other. As the wave propagation part in HISWA is modeled linearly and also the non-linear interaction source term has not been included in the present model, it seems advisable not to include the effect of dissipation due to bottom friction in the source term for frequency change. This is the more advisable because the reduction in wave period is mostly too large. It is stressed that in the present verification the effect of dissipation due to both bottom friction and wave breaking on the frequency change has been included.

For the semi-cylindrical bar geometry the standard setting of the wave breaking parameter together with the too low bottom friction factor fw did give much less accurate results than was obtained for the fully cylindrical bar. This has been shown to be due to the generation of wave-induced currents in the wave basin for this geometry; it has been argued that wave-induced currents are of much less importance in the fully cylindrical bar geometry because of the symmetric situation. The measured current field (for measurements me35) has been introduced in HISWA and the effect of inclusion of current refraction gave a large improvement in performance. It was also shown that some improvement could be obtained by taking a higher wave breaking parameter, but inclusion of current refraction was more effective. In the case of accounting for current refraction the bias is -4 % and the root mean square error, rmse, is 5.5 %. Comparison with the corresponding case for the fully cylindrical bar shows about the same rmse and a somewhat larger negative bias.

The general conclusion for the capabilities of the wave height prediction of HISWA in the present laboratory situation is that the wave height are predicted excellently.

The wave period.

The experiments have not been set up especially for testing the performance
of the wave period prediction and indeed this aspect of HISWA can also be
tested better in a one-dimensional situation such as is encountered in a
wave flume. Because the fully cylindrical bar geometry is effectively such
a one-dimensional situation with the added feature of directional spread-
ing, these experiments are suited for getting some idea of the wave period
prediction. As HISWA uses a very uncommon mean wave frequency, standard
wave data processing programs do not yield this measure standardly. The
wave period has therefore only been computed from the measured variance
densities at the locations where also the wave direction and the direc-
tional spread have been evaluated. Because three of these sites are situ-
ated in front of the bar and three are situated behind the bar, the general
picture of performance can be obtained from the present measurements.

The result for the fully cylindrical bar is that, except for the low wave
height case, the predicted wave period is 30 % too low compared with the
corresponding measure obtained from the variance densities. As this bar-
typed bottom geometry is a very simple one because no other bottom varia-
tions are present and only a very localized wave breaking zone is present,
the result is not good. One has to remember that such far too large changes
in wave period do have much influence on the wave propagation characteris-
tics in realistic two-dimensional situations. In this connection it has to
be noted that the deviations in T give even an optimistic view of the situ-
ation. When considering the more fundamental frequency and defining the
relative deviation in the usual way, deviations of order 50 % are obtained
(consider as an example computation ve25 for site 38 : for T we have -33.7
% and for f we have +50.9 %).

The wave frequency change in HISWA is based on a similarity approach of the
variance density in k-space; a too simple spectral shape has been taken.
The measurements show that considerable breaking over an underwater bar re-
sult in a double peaked spectrum (see Figures 6-8). The same behaviour is
found in prototype measurements, e.g. in the Haringvliet region due to wave
breaking over the Hinderplaat, see Fig. 18 in Dingemans et al. (1984) or
Figs. 62 in Dingemans (1983). It is nearly impossible to identify in such
wave spectra a single characteristic wave frequency. Indeed, one can always
compute some mean wave frequency from such spectra by some algorithm, but

that does not guarantee the representiveness of the computed mean frequency
for the total of the wave behaviour. Most of the spectra E(f) have two dis-
tinct peaks suggesting that it might be possible to represent the wave
spectra after a breaking zone by two wave systems with distinct frequen-
cies. It is stressed that the second peak in the variance density is
generally not a second harmonic of the first peak. It is therefore no
wonder that HISWA cannot predict the wave frequency accurately in such a
situation in which not one but two representative frequencies are present.

The situation of a near-shore region without bars and more or less uniform-
ly decreasing in water depth in coastwards direction was not investigated
by us. Such coastal regions are often characterized by a very mildly slo-
ping bottom topography and consequently a spatially extensive region in
which wave breaking occurs might be expected. The effect of a too large
reduction in wave period on the wave heights can be estimated qualitatively
as follows. In the wave breaking formulation of Battjes and Janssen (1978)
and Battjes and Stive (1985) the maximum allowable wave height Hm plays a
crucial role. Because of the increase in frequency the wave number increa-
ses also and the effect is a reduction of Hm leading to increased wave
breaking (increased in relation to the fixed frequency case) which in it-
self is a reason for further increase of frequency. Furthermore, the dissi-
pation function due to wave breaking is also linearly dependent on the fre-
quency, see also appendix U. This sequence may lead to an instability in
that the wave height prediction is increasingly too low. A higher, but
fixed, wave breaking parameter is expected not to be sufficient for a good
wave height prediction in the whole domain. The result on the wave heights
is a faster reduction in the wave breaking zone than is obtained with fixed
frequency wave propagation models. This in itself is no reason to reject
the predictions made with HISWA in such mildly sloping near-shore regions.
Indications of a too fast reduction in wave height in such mildly sloping
regions have recently been obtained (November 1987) in a project at Delft
Hydraulics. It has to be remarked that there the influence of wind has also
been taken into account. The general picture of the wave height distri-
bution is very good, but the wave period reduction is indeed rather large.
However, no measurements are available in that situation to test this
qualitative description.

The general conclusion for the wave frequency prediction is that the model-
ing of the change in frequency needs further attention.

Principal wave direction.

The performance of the prediction of the principal wave direction is best tested in the situation of the semi-cylindrical bar geometry. It has been shown that for the standard computations ve3x for that situation the wave direction prediction was rather inaccurate. The reason has been shown to lie in the neglection of current refraction effects due to the wave-driven currents. When current refraction is accounted for, the performance of the computed principal wave directions is greatly increased, but nonetheless, still deviations of 6 to 7° are present behind the bar. For the measured directions errors up to 4° are present as follows from the fully cylindrical bar situation. The statistical parameters show a less satisfactory performance for the prediction of the wave directions, but this may well be caused by the fact that in that comparison the measured values are supposed to be error-free, while the measurement errors in the wave directions are considerably larger than those for the surface elevation.

The numerical accuracy of the computation of wave directions has been investigated to some extent from the computed values in the fully cylindrical bar situation. This accuracy was shown to depend on the step size used in discretizing the direction in relation to the directional spreading parameter σ. The rate $\sigma/d\theta$ has to be chosen large enough and a value larger than 3 is recommended.

Directional spread.

A few results for the intercomparison of the spectral spreading from the computations and the measurements have been presented. This comparison should be taken not too strict because of the different measures used for spectral spreading in both cases. Only the trend in computations and measurements is relevant here. Different behaviour is found for the computations in relation to the measurements. This has been explained by simple refraction analysis arguments. In HISWA the wave frequency is locally nearly the same for the various directions sothat refraction induces a decrease in the spread. In the measurements we have a truly two-dimensional spectrum and refraction analysis shows that waves of different frequency starting in the same direction do travel after some distance in different directions. So in the measurements opposing effects are at work while in

the computations only one effect is active. For the wide directional dis-
tributions the measurements show a nearly constant directional spreading,
while the computations show much more variation, although consistent with
refraction analysis. Because of the parametrization in frequency as is ap-
plied in HISWA, it is not possible to predict the natural behaviour of the
directional spreading accurately.

Recommendations.

In this section we present a few suggestions which might improve the per-
formance of HISWA in some aspects. Foremost the problem of the change in
wave frequency due to dissipative processes has to be studied.

1. *Wave frequency change.*

In the first place a distinction has to be made for those situations where
the wave spectra may be considered to be uni-modal and those where the uni-
modality is clearly not the case.

For mildly sloping bottom geometries the assumption of uni-modality of the
variance density seems a reasonable one, at least up to a certain distance
from the coast. Similarity of wave spectra in k-space could perhaps be a
useful approach but the problem remains how to distribute the dissipation
over the spectral range. This is the crucial part in the process on which
the success of the frequency change rests. At least a realistic form of the
spectrum in k-space should be adopted because the presently chosen simple
form does not do the job satisfactory. It might be that such a more real-
istic form does give better predictions of the wave frequency, but a funda-
mental approach of the problem is expected to give better results in the
long run.

On deep water the problem is relatively simple because the maximum wave
steepness gives a relation between wave height and wave frequency. The pro-
gram HISWA has its field of application especially in near-shore areas and
thus a solution has to be found for those applications.

For the bar-typed bottom geometries we are presently working out some ideas
for the frequency prediction behind the dissipation zone and results will
appear elsewhere.

2. Directional distribution.

We had some difficulties in defining the same kind of directional distribution in both measurents and computations; this was due to the fact that in both instances only the definition of the distribution according to a single type of function was possible. In HISWA only the $\cos^m \theta$ type of distribution is possible and in the wave generation only the distribution $\cos^{2s}(\theta/2)$ is possible (see Eqs. (F.11) and (F.26)). It is advisable to make it possible also to use different types of directional distributions in HISWA sothat the connection with possibly available data can be made easily and objectively for projects to be carried out with HISWA. We suggest to program also the cases of the $\cos^{2s}$ model and the case of the wrapped normal distribution.

3. Boundary conditions.

As in the HISWA version available to us for the present study effectively only fully dissipating bounadary conditions were available for the sidewards boundaries, the comparison with measurements with effects of reflections from the sidewalls was more difficult than would have been necessary when also the possibility of applying (partially or fully) reflecting boundary conditions. Furthermore, it would be nice if also socalled weakly reflecting boundaries could be imposed, but the directionality of the waves poses here a serious problem.

4. The performance of HISWA on mildly sloping bottoms.

As discussed before, the performance of HISWA on mildly sloping bottom geometries, with large wave breaking zones has not been verified to our knowledge. Remark that the Haringvliet region is not suited for this purpose. We expect that the measurements taken some years ago at Egmond might be useful for this purpose. We suggest to perform a few tests for that area, especially to see the behaviour of the wave period and the decrease of wave height in the dissipation zone. We are aware of the fact that also in the Egmond area bar-typed bottom profiles are present, but we think they have less influence than the Hinderplaat in the Haringvliet region; this has to be checked first.

5. *A check of HISWA on the shoal experiment.*

It would be interesting to check the performance on the data of the shoal experiment (see Berkhoff et al., 1982, or Dingemans, 1985). The effect of caustic regions on the performance of HISWA could then be ascertained. Notice that for CREDIZ the inclusion of the non-linearity on the wave celerity was seen to have much influence on its performance, see Dingemans and Radder (1986). It is to be seen whether HISWA performs significantly better in these regions than the wave ray model STROBO.

6. *Compilation of verification results of HISWA for different situations.*

It seems to be advisable for future project work to be carried out with the HISWA program to make a short compilation of the various situations in which computations with HISWA have been compared to measurements. This is especially of importance because the findings of the wave period performance are sometimes in conflict with each other. So, in the Haringvliet region, the predicted wave period is too large (as noted in Holthuijsen and Booij, 1986), whereas we find too low wave period predictions in the present study.

REFERENCES

Battjes, J.A. (1974)
Computation of set-up, longshore currents, run-up and overtopping due to
wind generated waves.
Thesis, Delft University of Technology, June 1974

Battjes, J.A. and J.P.F.M. Janssen (1978)
Energy loss and set-up due to breaking random waves.
Proc. 16th Int. Conf. on Coastal Eng., Hamburg 1978 pp. 569-587

Battjes, J.A. and M.J.F. Stive (1985)
Calibration and verification of a dissipation model for random breaking waves.
J. of Geophysical Research 90(C5), Sept. 1985 pp. 9159-9167

Battjes, J.A., T.J. Zitman and L.H. Holthuijsen (1986)
A re-analysis of the spectra observed in JONSWAP.
Proc. 20th Int. Conf. on Coastal Eng., Taipei, Nov. 1986 pp. 17-26

Berkhoff, J.C.W., N. Booij and A.C. Radder (1982)
Verification of numerical wave propagation models for simple harmonic
linear water waves.
Coastal Engineering 6, 1982, pp. 255-279

Booij, N., L.H. Holthuijsen and T.H. Herbers (1985)
A numerical model for wave boundary conditions in port design.
Int. Conf. on Numerical and Hydraulic Modelling of Ports and Harbours,
Birmingham, England, April 1985, pp. 263-268

Dingemans, M.W. (1981)
Surface wave propagation over an uneven bottom;
spectral calculations of refraction over a shoal.
Delft Hydraulics Laboratory, Report W301 part 3, November 1981

Dingemans, M.W. (1983)
Verification of numerical wave propagation models with field measurements;
CREDIZ verification Haringvliet.
Delft Hydraulics Laboratory, Report W488 part 1, December 1983

Dingemans, M.W. (1985)
Surface wave propagation over an uneven bottom;
evaluation of two-dimensional horizontal wave propagation models.
Delft Hydraulics Laboratory, Report W301 part 5, December 1985

Dingemans, M.W. and A.C. Radder (1986)
Surface wave propagation over an uneven bottom;
wave deformation by a shoal; effect of non-linearity.
Delft Hydraulics Laboratory, Report W301 part 6, October 1986

Dingemans, M.W., M.J.F. Stive, J. Bosma, H.J. de Vriend and J.A. Vogel (1986)
Directional nearshore wave propagation and induced currents.
Proc. 20th Int. Conf. on Coastal Eng., Taipei, Nov. 1986 pp. 1092-1106

Dingemans, M.W., M.J.F. Stive, A.J. Kuik, A.C. Radder and N. Booij (1984)
Field and laboratory verification of the wave propagation model CREDIZ.
Proc. 19th Int. Conf. on Coastal Eng., Houston, 1984 pp. 1178-1191

Goda, Y. (1985)
Random seas and design of maritime structures.
University of Tokio Press, 1985 323 pp.

Gradshteyn, I.S. and I.W. Ryzhik (1965)
Table of integrals series and products.
Academic Press, New York and London 1965, fourth edition, 1086 pp.

Holthuijsen, and N. Booij (1986)
A grid model for shallow water waves.
Proc. 20th Int. Conf. on Coastal Eng., Taipei, Nov. 1986 pp. 261-270

Jonsson, I.G. (1978)
A new approach to the oscillatory rough turbulent boundary layers.
ISVA, Techn. Univ. of Denmark, Series Paper 17, 1978

Jonsson, I.G. (1980)
A new approach to the oscillatory rough turbulent boundary layers.
Ocean Engineering 7(1) , 1980 pp. 109-152

Kinsman (1965)
Wind waves, their generation and propagation on the ocean surface.
Prentice-Hall, Inc., Englewood Cliffs, N.J. 1965 676 pp.

Kostense, J.K., K.L. Meijer, M.W. Dingemans,
A.E. Mynett and P. van den Bosch (1986)
Wave energy dissipation in arbitrarily shaped harbours of variable depth.
Proc. 20th Int. Conf. on Coastal Eng., Taipei, Nov. 1986 pp. 2002-2016

Longuet-Higgins, M.E. (1956)
The refraction of sea waves in shallow water.
J. of Fluid Mech. 1(2) , 1956 pp. 163-176

Longuet-Higgins, M.E. (1975)
On the joint distribution of the periods and amplitudes of sea waves.
J. of Geophysical Res. 80(18) , June 1975 pp. 2688-2694

Longuet-Higgins, M.E., D.E. Cartwright and N.D. Smith (1961)
Observations of the directional spectrum of sea waves using the
motions of a floating buoy.
Proc. Conf. Ocean Wave Spectra, 1961 pp. 111-132

Mynett, A.E., J. Bosma and P. van Vliet (1984)
Effects of directional seas in coastal regions.
Symposium on Description and Modelling of Directional Seas, Paper B7,
Lyngby, Denmark

Ochi, M.K. (1982)
Stochastic analysis and probabilistic prediction of random seas.
Advances in Hydroscience, Vol. 13, 1982 pp. 217-375

Officier, M.J., C.B. Vreugdenhil and H.G. Wind (1986)
Application in hydraulics of numerical solutions of the Navier-Stokes
equations.
in : Computational techniques for fluid flow (Eds.C. Taylor, J.A. Johnson
and W.R. Smith) pp. 115-147, Peneridge Press, Swansea, U.K., 1986

Olver, F.W.J. (1974)

Asymptotics and special functions.

Academic Press, New York and London 1974,   572 pp.

Rice, S.O. (1944)

Mathematical analysis of random noise.

Bell System technical Journal 23, 1944, pp. 282-332

Sand, S.E. and A.E. Mynett (1987)

Directional wave generation and analysis.

presented at the IAHR Seminar on wave analysis and generation in laboratory

basins, held in Lausanne, August 1987

Stive, M.J.F. and M.W. Dingemans (1984)

Verification of a one-dimensional wave energy decay model.

Delft Hydraulics laboratory, Report M1882-1, December 1984

Vanmarcke, E. (1983)

Random fields : analysis and synthesis.

The MIT Press, Cambridge, Ma. 1983   382 pp.

Willmott, C.J. (1981)

On the validation of models.

Physical Geography 2 (2), 1981 pp. 219-232

Willmott, C.J. (1984)

On the validation of model performance in physical geography.

in : Spatial statistics and models (Eds. G.L. Gaile and C.J. Wilmott),

pp. 443-460, Reidel 1984

Willmott, C.J., S.G. Ackleson, R.A. Davis, J.J. Feddema, K.M. Klink,

D.R. Legates, J. O'Donnell and C.M. Rowe (1985)

Statistics for the evaluation and comparison of models.

J. of Geophysical Research 90(C5), Sept. 1985 pp. 8995-9005

Zitman, T.J. (1985)

A re-analysis of the JONSWAP data.

Master's Thesis, Delft University of Technology,

Civil Eng. Department, Dec. 1985

de voorst office
voorsterweg 28
marknesse

p.o. box 152
8300 ad emmeloord
the netherlands

telephone (31) 5274-2922
telex 42290 hylvo-nl
telefax (31) 5274-3573

amsterdam ■

main office
rotterdamseweg 185
delft

p.o. box 177
2600 mh delft
the netherlands

telephone (31) 15-569353
telex 38176 hydel-nl
telefax (31) 15-619674

delft hydraulics
consultancy & research